PHONON MEAN FREE PATH AND THERMAL CONDUCTIVITY ANALYSIS OF WIDE AND ULTRA-WIDE BANDGAP MATERIALS

by

Esra İlke Albar

B.S., Mechanical Engineering, Boğaziçi University, 2017

Submitted to the Institute for Graduate Studies in
Science and Engineering in partial fulfillment of
the requirements for the degree of
Master of Science

Graduate Program in Mechanical Engineering
Boğaziçi University

2020

ACKNOWLEDGEMENTS

I would like to express my gratitude to Dr. Nazlı Dönmezer, who is the greatest mentor and advisor a student can have. I am grateful to my dear father Recep Albar, my beloved mother Perihan Albar and my wonderful sister Özge Albar. They always supported me with their endless love.I would also like to thank my colleagues Haluk Kundakçıoğlu, Canberk Dündar and other MinTh LAB members. I am also grateful to my dear friends Duru Su Kadıoğlu,Batıbey Batmacı, Alev Ecevitoğlu and Erman Kayhan for their immense support. Finally, I thank Boğaziçi University Research Funding (BAP) Organization for their support of our work with grant number 14430. Their fund made this thesis possible.

ABSTRACT

PHONON MEAN FREE PATH AND THERMAL CONDUCTIVITY ANALYSIS OF WIDE AND ULTRA-WIDE BANDGAP MATERIALS

As the Knudsen number (defined as the as the ratio of the molecular mean free path length to length scale of the device) increases, materials' thermal properties are compromised due to disruption of phonon movement. If the thermal conductivity and mean free path relationship of the phonons is known, interference of size effects at small scales can be predicted as well as thermal conductivity reductions. To do this, thermal accumulation spectra of four wurtzite semiconductor materials: gallium nitride, aluminum nitride, aluminum gallium nitride, and beta form gallium oxide were calculated at different temperatures. As these materials are usually employed in high power electronic applications in confined structures, a method was devised in order to infer their conductivities at small scales from accumulation spectra. Third-order force constants, which are the expanded coefficients of crystal ground energy, are used directly for mentioned calculations.It was observed that this approach is very useful at high anharmonicity where MFP range is short and temperature is high. This work concluded that MFP spectra contributing to thermal conductivity were 1661.7 nm, 1648.8 nm, 442.3 nm and 467.3 nm respectively for GaN, AlN, $AlGaN$ and β-form Ga_2O_3 at 300 K. Hence, size effects are expected to dominate conductivity at scales smaller than these values.

ÖZET

YÜKSEK VE ULTRA-YÜKSEK BANT ARALIKLI MALZEMELERİN FONON ORTALAMA SERBEST YOL VE ISIL İLETKENLİK ANALİZİ

Moleküler ortalama serbest yolun, cihaz karakteristik uzunluğuna oranı olarak tanımlanan Knudsen sayısı arttıkça, fonon hareketinin engellenmesi sonucu malzemenin ısıl özelliklerinde kayıp yaşanır. Eğer fononların ısıl iletkenlik ve ortalama serbest yol(OSY) ilişkisi bilinirse, malzemedeki boyut etkileri ve kaybedilen ısıl iletkenlik miktarı tahmin edilebilir. Bu amaçla, dört würtzit yarıiletken malzeme: galyum nitrat, alüminyum nitrat, alüminyum galyum nitrat ve beta form galyum oksit için ısıl iletkenlik birikimi farklı sıcaklıklarda hesaplanmıştır. Bu malzemeler çoğunlukla yüksek güç elektroniği uygulamalarında, küçük ve kısıtlı boyutlarda kullanıldıklarından, ısıl iletkenlik birikim grafiğinden küçük boyutlarda karşılaşılan iletkenlik miktarının elde edilebilmesi için bir yöntem geliştirilmiştir.Kristal enerjisinin Üçüncü dereceden güç katsayıları bu hesaplamalarda kullanılmıştır. Bu yaklaşımın anharmonikliğin arttığı kısa OSY ve yüksek sıcaklık durumlarında kullanışlı olduğu anlaşılmıştır. Isıl iletkenliğe katkıda bulunan en büyük OSY değerleri GaN, AlN, $AlGaN$ ve β-form Ga_2O_3 için sırasıyla 1661.7 nm, 1648.8 nm, 442.3 nm and 467.3 nm olarak hesaplanmıştır. Boyut etkilerinin, bu uzunluklardan daha küçük cihaz boyutlarında gözlemlenmesi beklenmektedir.

TABLE OF CONTENTS

LIST OF FIGURES

LIST OF TABLES

LIST OF SYMBOLS

c	Specific heat
C	Spring constant
$\hbar$	Reduced Planck constant
k	Thermal conductivity
k_b	Boltzmann constant
L	Characteristic Length
n	Phonon equilibrium occupation number
N	Number of unit cells in sample
q	Wavevector
r	Spatial variable
T	Temperature in K
u	Displacement
U	Particle energy
v	Phonon Group Velocity
V_0	Volume of unit cell
Γ	Inverse phonon lifetime
Λ	Mean Free Path
τ	Relaxation time
Φ	Crystal energy
Ψ	Wave function
ω	Frequency

LIST OF ACRONYMS/ABBREVIATIONS

2D	Two dimensional
2DEG	Two dimensional electron gas
3D	Three dimensional
ALD	Atomic Layer Deposition
ALE	Atomic Layer Epitaxy
AlGaN	Aluminum Gallium Nitride
AlN	Aluminum Nitride
BB-FDTR	Broadband Frequency Domain Thermoreflectance
BFOM	Baliga Figure of Merit
BTE	Boltzmann Transport Equation
DFT	Density Functional Theory
DUV	Deep Ultraviolet
EQE	External Quantum Efficiency
FC2	Second Order Force Constants
FC3	Third Order Force Constants
FDTR	Frequency Domain Thermoreflectance
finFET	Fin Field Effect Transistor
GaN	Gallium Nitride
HCP	Hexagonal Closed Pack
HEMT	High ELectron Mobility Transistor
HVPE	Hydride Vapor Phase Epitaxy
Kn	Knudsen Number
LED	Light Emitting Diode
MD	Molecular Dynamics
MFP	Mean Free Path
MOCVD	Metal Organic Chemical Vapor Deposition
MODFET	Modulation Doped Field Effect Transistor
MOSFET	Metal Oxide Semiconductor Field Effect Transistor

MOVPE	Metal Oxide Vapor Phase Epitaxy
NEMD	Non Equilibrium Molecular Dynamics
PAW	Projector Augmented Wave
PLD	Pulsed Laser Deposition
RF	Radio Frequency
SCF	Self Consistent Field
TCO	Transparent Conducting Oxide
TDD	Threading Dislocation Density
TDTR	Time Domain Thermoreflectance
TTI	Thermoreflectance Imaging
UV	Ultraviolet
UWBG	Ultra Wide Band Gap
VASP	Vienna Ab-initio Simulation Package
WBG	Wide Band Gap

1. INTRODUCTION

1.1. Wide and Ultra-Wide Bandgap Materials

Wide and Ultra-wide bandgap (WBG and UWBG) semiconductor materials have electronic bandgaps of 3.4 eV or higher and have outstanding properties such as high breakdown field, high electron velocity and good thermal stability at high frequencies. As Figure 1.1 demonstrates, WBG and UWBG materials represent strong alternatives to commonly used silicone devices.

Due to their large bandgap and other listed properties, WBG and UWBG materials are frequently employed in power electronic and opto-electronics applications such as high electron mobility transistors(HEMT), light-emitting diodes(LED), and lasers. Figure 1.2 shows some of these applications.

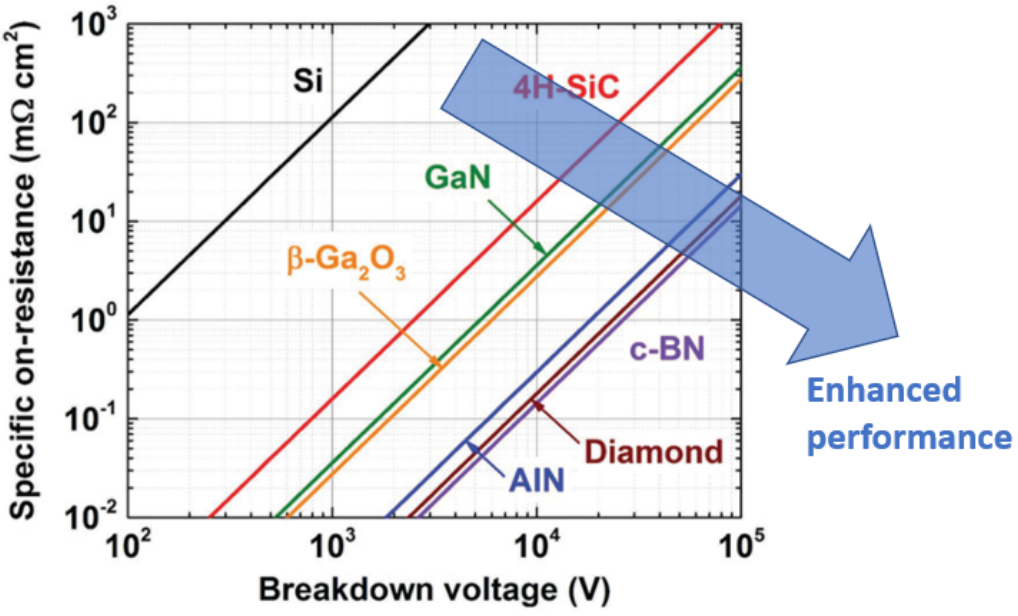

Figure 1.1. Specific on-resistance vs Breakdown voltage of WBG and UWBG materials [1]. This relation indicates a materials' potential for power switches.

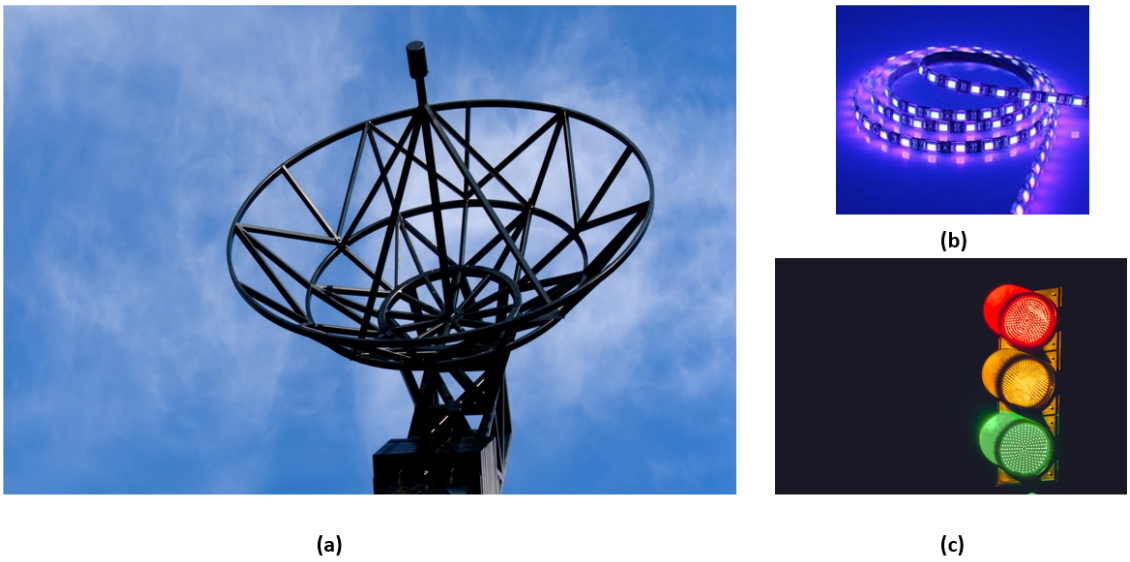

Figure 1.2. UWBG materials are used in (a) HEMT's in radars, (b) DUV light production, (c) LED traffic lights.

Gallium nitride (GaN) , aluminum nitride (AlN), aluminum gallium nitride ($AlGaN$), and β-form gallium oxide (Ga_2O_3) are examples of wide and ultra-wide bandgap semiconductor materials. All four of these materials share the wurtzite structure (which is a hexagonal closed pack form) which is visible in Figure 1.3 and are semiconductors, however, they all have unique properties. Especially, described as ultra-wide bandgap materials, high Al-including $AlGaN$ and Ga_2O_3 are expected to provide new opportunities in near future in terms of deep ultraviolet(DUV) optoelectronics, quantum information, and extreme-environment applications [1]. It is reported that replacing Si in power electronics applications with alternatives such as GaN and $\beta - Ga_2O_3$ promises environmental benefits of both decreasing CO_2 emission and saving energy [2,3]. In this section, the properties of all four materials: Gallium nitride (GaN), aluminum nitride(AlN), aluminum gallium nitride ($AlGaN$), and β-form gallium oxide (Ga_2O_3) will be briefly introduced.

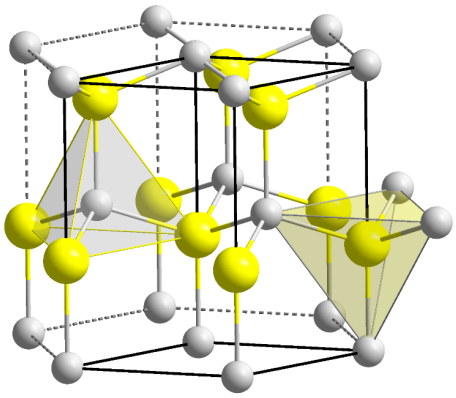

Figure 1.3. A schematic of wurtzite structure.

1.1.1. Gallium Nitride (GaN)

As a popular wide bandgap semiconductor, GaN is defined as the threshold between wide-bandgap and ultrawide bandgap materials with its bandgap of 3.4 eV [1]. This work examines its wurtzite form, which is also a stable hexagonal closed pack (HCP) form [4]. Crystal structure of GaN is represented in Figure 1.4. Wurtzite GaN thin films are frequently grown via metal organic chemical vapor deposition (MOCVD), metalorganic vapor-phase epitaxy (MOVPE) [5], molecular beam epitaxy (MBE) and also pulsed laser deposition (PLD) [6].

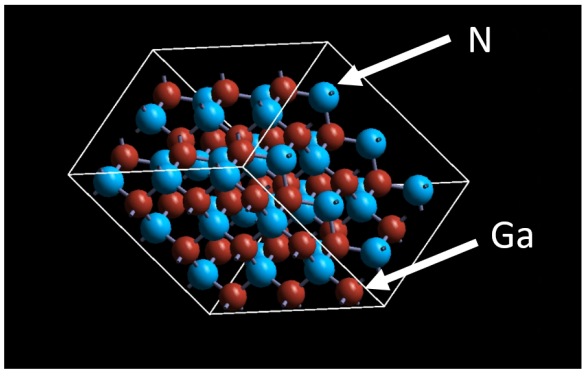

Figure 1.4. Crystal structure of GaN.

GaN is used in power electronics applications [2, 7, 8] due to its high bandgap, large breakdown voltage, low dielectric constant and higher thermal stability as well as its high melting point leading to its sustainability in both economic and environmental perspectives [9]. GaN is perceived as a solution for more effective power conversion, paving the way to better motor drives, charger technologies and enhanced power factor correction [9–11]. When coupled with $AlGaN$; GaN layer permits the formation of two-dimensional electron gas (2DEG) [10, 12, 13] which corresponds to an extreme electron mobility leading to an immense current density in HEMT devices.

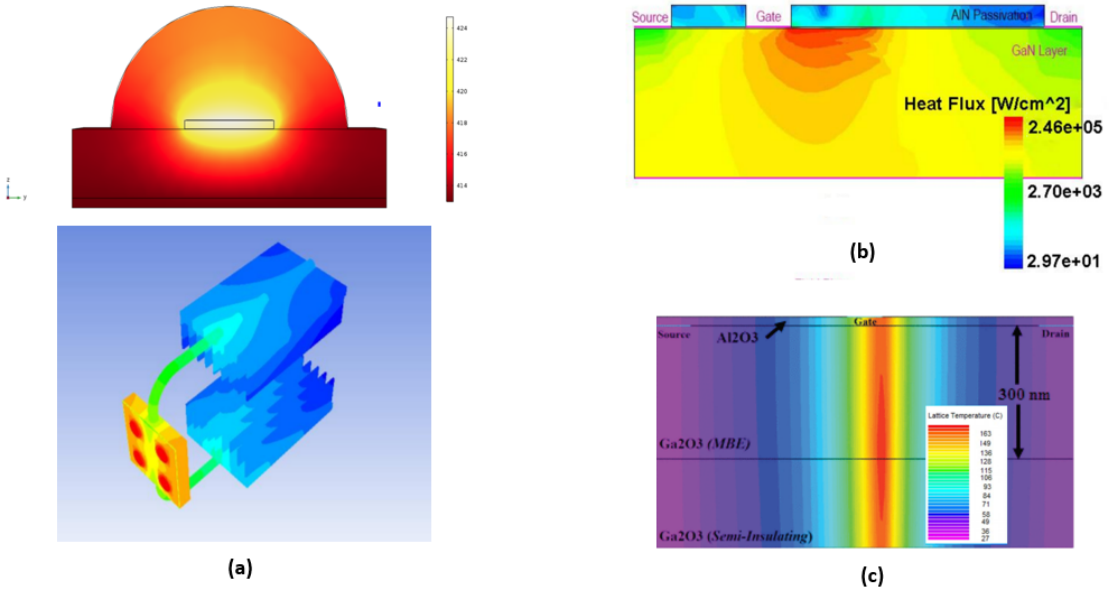

Figure 1.5. Cross-sectional schematics visualizing heating of (a) A high power LED package [14] (b) GaN HEMT [15] (c)A $\beta - Ga_2O_3$ MOSFET scheme visualizing localized heating in structure [16].

Other prevalent areas of employment for GaN are opto-electronics [17], blue/ultraviolet (UV) LED technology and UV Sensors [18], and data storage solutions [19]. Electric vehicles, solar and wind power generation, communication technologies and aerospace applications are all to benefit from the usage of GaN [10]. A simple schematic example of these devices is visible in Figure 1.5. As seen in Figure 1.5, heating is a major drawback of these devices since they are operated at high powers and high frequencies.

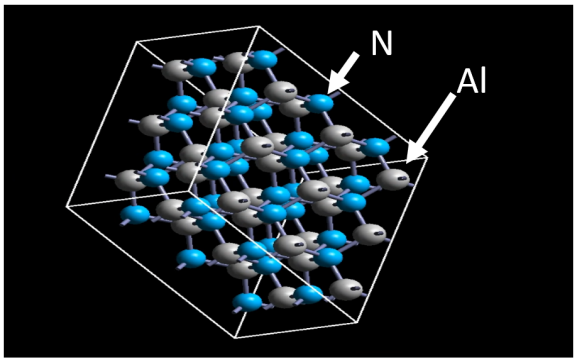

Figure 1.6. Crystal structure of AlN.

1.1.2. Aluminum Nitride (AlN)

Aluminum nitride (AlN) is another popular Group III-V nitride material. Crystal structure of AlN is represented in Figure 1.6. There exists a great variety of methods of AlN thin film manufacturing such as reactive magnetron and direct current (DC) sputtering [20, 21], pulsed laser ablation, MOCVD and MBE [22]. Extensive literature focus on threading dislocation density (TDD) studies on AlN thin film samples also hints at its popularity [23–25].

Due to its unique properties such as high thermal conductivity [26], large (up to 6.42 eV, which renders it a UWBG material) bandgap [27], high electrical insulation, capacity of metallization and its low thermal expansion coefficient, AlN is frequently employed in electronics applications. AlN is employed in trending applications such as HEMT , Ultra Violet Light Emitting Diodes (UV-LED's), and microwave filters [28–31]. Especially, UV and DUV devices present an important motivation in AlN production since this technology employs this material as both the substrate and the operating layer [32–34]. Applications of DUV technology extends to a variety of fields including water sterilization and optical instrumentation [35,36]. Most importantly, DUV LED's are expected to replace gas lasers and mercury lamps which is expected to benefit the environment greatly [34, 37]. Such applications are shown in Figures 1.1 and 1.2. As it is described in Figure 1.5, these applications are susceptible to localized heating due to phonon confinement.

1.1.3. Aluminum Gallium Nitride ($AlGaN$)

Aluminum gallium nitride ($AlGaN$) is an alloy of previously mentioned materials AlN and GaN. It is usually noted as $Al_xGa_{1-x}N$ where x denotes the Al fraction. Unit cell representation of $AlGaN$ is shown in Figure 1.7. $AlGaN$ is a unique material in terms of its properties being tunable due to the Al fraction in the alloy [38, 39]. As a member of group III-V materials, $AlGaN$ is grown via MBE, MOCVD, reactive sputtering, and occasionally hydride vapor phase epitaxy (HVPE) and organometallic vapor phase epitaxy (VPE) [39–41].

Due to its high saturation drift velocity, resistance to high temperature, high breakdown voltage [42], small thermal expansion coefficient, corrosion resistance and, as it is previously mentioned, formation of two dimensional electron gas (2DEG) at $AlGaN/GaN$ interface layer, $AlGaN$ is frequently used in $AlGaN/GaN$ HEMTs, and modulation-doped field effect transistors (MODFET) [13, 43–47]. Since $AlGaN$ has a direct bandgap like AlN and GaN, unlike indirect bandgap semiconductors such as silicon, electron transition to conduction band occurs directly. Thus, this process does not require an interference of a phonon for additional quasi-momentum. Moreover $AlGaN$ layers reportedly permits the reduction of optical losses and enhancement of external quantum efficiency (EQE) [33, 48]. This leads to $AlGaN$ dominance in opto-electronic devices such as edge and surface emitting lasers and UV/DUV LEDs [48,49]. Some examples of such applications are shown in Figure 1.2.

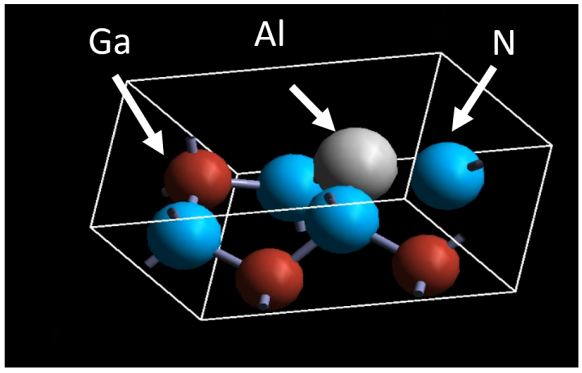

Figure 1.7. Unit cell of $AlGaN$.

Briefly, $AlGaN$ devices are popularly used in both high-power electronics and DUV-LEDs due to its multiple benefits. Similar to devices made of GaN and AlN, these devices are also frequently operated at high frequencies and at high temperature, hence they are subjected to heating problems.

1.1.4. Beta Form Gallium Oxide (β-form Ga_2O_3)

The most stable and most preferred form of Ga_2O_3 is β-form amongst five other polymorphs [50]. β-form Ga_2O_3 is stable through the temperature spectrum up to its high melting point, hence $\beta - Ga_2O_3$ devices are also expected to stand against thermal fatigue [50]. Unit cell representation of β-form Ga_2O_3 is shown in Figure 1.8.

When it comes to thin film $\beta - Ga_2O_3$ production, there are a variety of methods. Magnetron sputtering is a preferred option [51], and is followed by MOCVD, MBE, VPE,PLD, atomic layer epitaxy (ALE) and atomic layer deposition (ALD) [3, 52]. These multiple methods and rapidly improving advances in $\beta - Ga_2O_3$ growth caused very high-quality single crystal samples at small costs with high success rates [3].

$\beta - Ga_2O_3$ has a large bandgap of 4.9 eV [3], hence it qualifies as a UWBG material [1]. Its advanced thermal and chemical stability, along with high breakdown field explains the extensive $\beta - Ga_2O_3$ usage in power electronics such as power switches

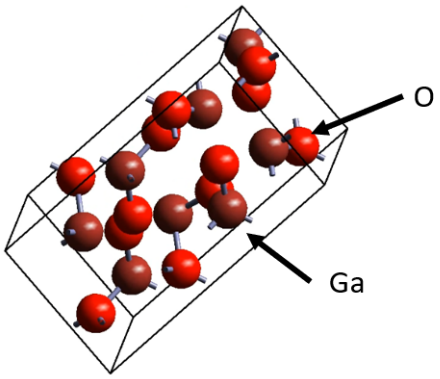

Figure 1.8. Unit cell of β-form Ga_2O_3.

and radio frequency (RF) devices. Namely, $\beta - Ga_2O_3$ is frequently employed in metal oxide semiconductor field effect transistors (MOSFETs) ,fin field-effect transistors (FinFETs), and Schottky diodes [52]. In power electronics, a way to evaluate the materials is Baliga Figure of Merit (BFOM) which is defined as the ratio of breakdown voltage to specific on-resistance. As seen in Figure 1.1, $\beta - Ga_2O_3$ has an enormous BFOM value (almost 4 times more than that of GaN) [52]. Therefore, $\beta - Ga_2O_3$ is excellent for power switches since it minimizes current leakage and energy losses. Also being a member of transparent conducting oxides (TCO), $\beta - Ga_2O_3$ offers excellent optoelectronics opportunities. It is employed in UV/DUV applications, especially solar blind UV detectors which are used to monitor UV emission levels as well as ozone layer thickness; and they are used in a variety of space applications [53, 54]. Finally, $\beta - Ga_2O_3$ structures are employed in several fields where they are subjected to harsh environments. As seen in the MOSFET in Figure 1.5, these group of applications are prone to heating problems due to size effects.

1.2. Thermal Issues and Size Effects

All applications of WBG and UWBG materials requires them to be used in small scale structures where phonons are trapped. To know the thermal conductivity of these micro and nano scale structures allows accurate modeling of device heating. Since these devices are already susceptible to heating problems as seen in Figure 1.5, a loss in conductivity due to confinement aggravates the results. For instance, once excessive heat is not successfully dissipated in HEMT shown in Figure 1.5, degradation of substrate due to high temperature is inevitable. Then, it is crucial to know the lost portion of thermal conductivity at that scale in order to avoid such failure. Not only the device's small scales, but also localization of the heating in form of hotspots as seen in Figure 1.5, restrict phonon movement. Then, size effects ensue. As confined structures such as thin films, nanowires, and hotspots do not have the same thermal conductivity as the bulk material, modeling of accumulation spectrum is required. Accumulation spectrum relates thermal conductivity to mean free path (MFP) value. Hence, it is possible to retrieve thermal conductivity of a structure at characteristic length level.

The aim of this work is to obtain thermal conductivity accumulation spectra of four WBG and UWBG materials in order to device a method to foresee thermal behavior of confined structures of these materials. Thermal conductivity at small scales can be retrieved from accumulation spectra. Thus, it becomes easier to tackle the problems caused by size effects. Finally, in order to understand size effects, it is important to understand how heat is transported at micro scale. Following section aims to define necessary concepts for this topic.

1.2.1. Phonons & Brillouin Zone

In semiconductors, heat is transmitted via lattice vibrations. These quantized lattice vibrations are defined as phonons. Phonons are characterized via their directions called wavevectors and amplitude of their frequencies. The relation expressing this is called the phonon dispersion relation. The equation that represents an example of phonon wavevector-phonon frequency in a chain containing two atoms of different masses is visible in Equation 1.1.

$$\omega(k) = \sqrt{\left(C\frac{(M+m)}{Mm} \pm C\sqrt{\frac{(M+m)^2}{M^2m^2} - \frac{4}{Mm}\sin^2\frac{ka}{2}} \right)} \tag{1.1}$$

Equation 1.1 is simply reached via modeling atomic vibrations as masses connected with a spring. Here, C is spring constant while $\omega(k)$ is the frequency associated with wavevector k. M and m correspond to masses of atoms in diatomic chain. When solved, eigenvalue problem in Equation 1.1 yields the curve in Figure 1.9. In Figure 1.9, one can observe two sorts of solutions: optic and acoustic solutions, representing optical and acoustic phonon modes. These solutions are stemming from the $\pm$ term in the equation, and their physical meaning is as follows: In optical mode, neighboring atoms move oppositely while in acoustic mode, these atoms move in harmony.

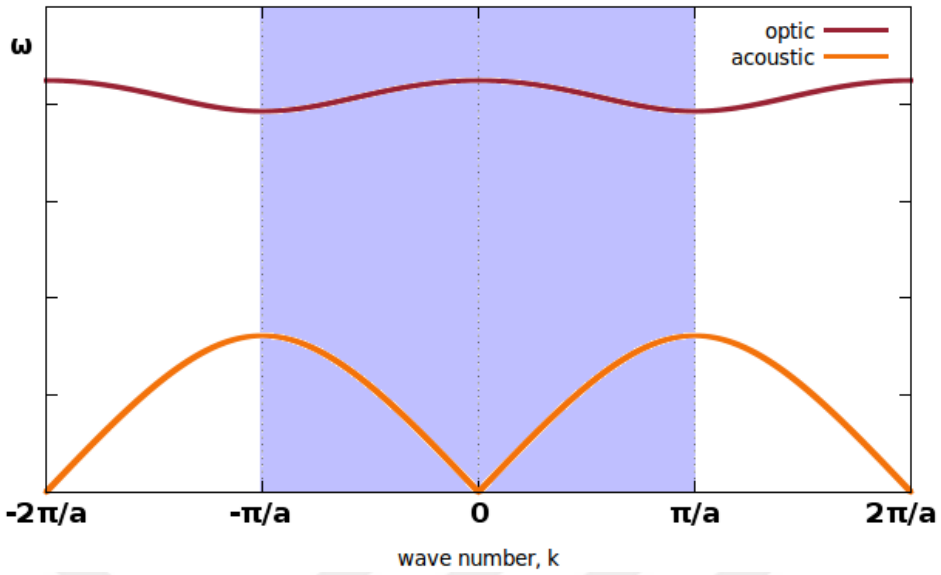

Figure 1.9. Phonon dispersion relation of diatomic chain [55].

If a three dimensional (3D) complex structure is in question, more optical and acoustic branches appear. Figure 1.10 visualizes a phonon dispersion graph of GaN obtained by Broido *et al.* [56].

As seen in Figure 1.10, in order to explain crystallographic directions better, certain specific notations (A, Γ, M, and K) are used. These notations are a part of Brillouin zone concept. As it is the primitive cell of the real space lattice (the arrangement of atoms in crystal), irreducible Brillouin zone is where lattice directions in phonon dispersion are expressed. First Brillouin zone of HCP structure, hence the directions noted in the phonon dispersion curve is visible in Figure 1.11.

1.2.2. Mean Free Path & Relaxation Time

Mean Free Path (MFP) is described as the path that a phonon can follow before colliding with another phonon or energy carrier. When thin films or structures with small dimensions, and/or localized heating are present, phonons' movement along its MFP is often disturbed, this problem is known as size effect. To understand whether size effects exist Knudsen number(Kn, defined as the ratio of phonon MFP (Λ) to

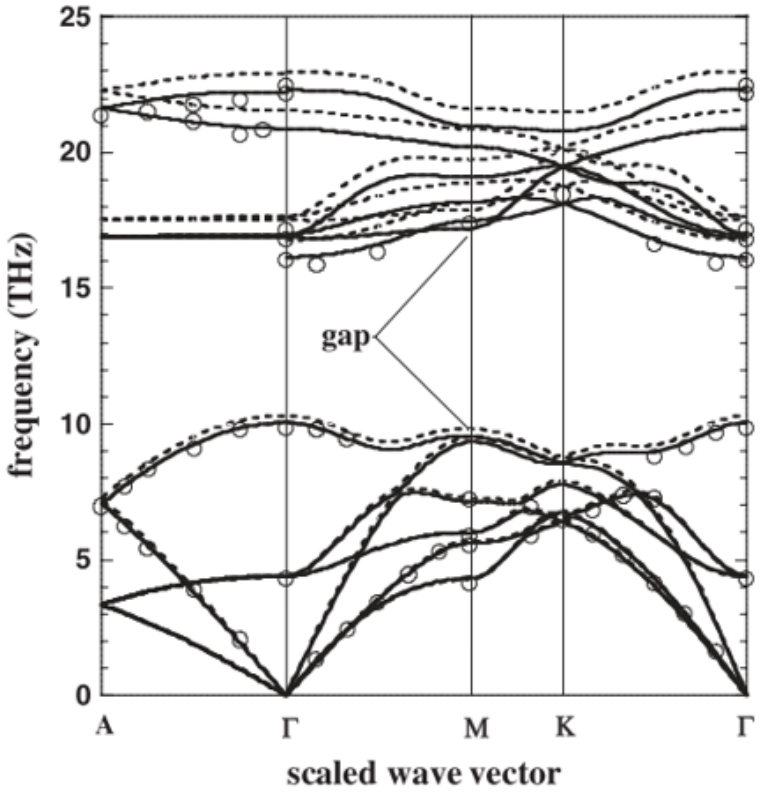

Figure 1.10. Phonon dispersion of wurtzite GaN obtained by Broido *et al.* [56].

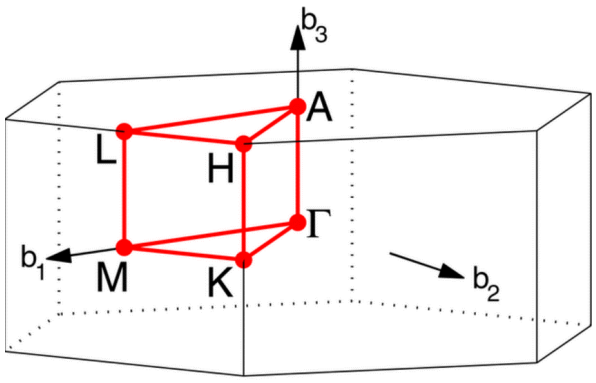

Figure 1.11. First Brouillin zone of HCP structure [57].

characteristic device length (L) as seen in Equation 1.2, is used. Characteristic length can be defined as the length of the device layer along which phonon travels. When $Kn > 1$, characteristic length is smaller than MFP of phonons and size effects are expected to dominate.

$$\text{Knudsen number} = \frac{\Lambda}{L} \tag{1.2}$$

As seen in Figure 1.12, if the path that a phonon can travel is constricted with the thin film length, phonon cannot convey its energy causing a loss in conductivity [58]. While a material sample has a spectrum of phonon MFP length, phonons with MFPs longer than their counterparts are likely to be restricted in small/thin structures as described in Figure 1.12. Trapped phonons then might cause heating and degradation. Moreover, not only thin films, but also localized heating may obstruct phonons' travel [13]. Then, this entrapment should also be considered in devices that are subjected to localized heating which suffers from small heating spots [59,60]. Finally, relaxation time is the time interval that covers phonon's travel until a collision. To model accumulated conductivity, one needs to define relaxation time as well as phonon MFP. Details of these definitions will be discussed further in calculation details.

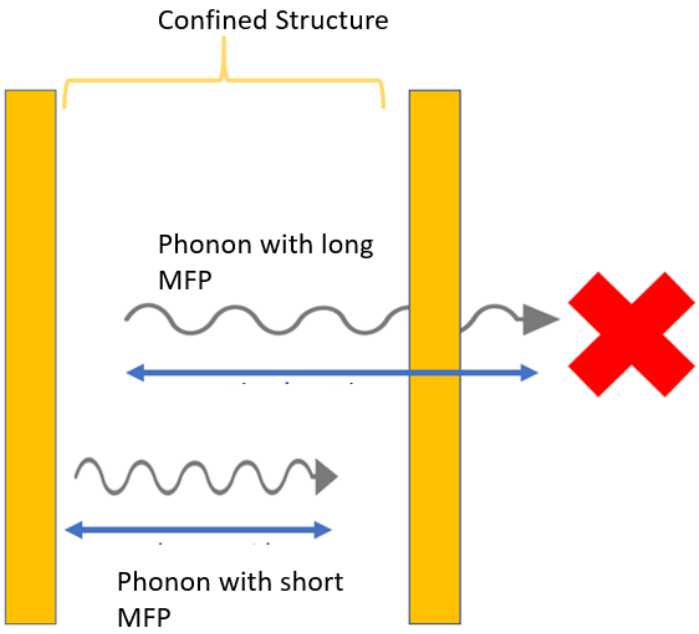

Figure 1.12. Phonon travel in confined structures, phonons with long MFP are obstructed.

1.3. Characterization of Thermal Size Effects

At small scales, thermal transport in materials behave differently than bulk materials due to thermal size effects. If one aims to design and utilize nano and micro scale devices, then one should be able to characterize thermal behavior at this scale. Researchers have been trying to characterize thermal size effects in devices subjected to localized heating and thin materials using experimental and theoretical approaches. This section summarizes these attempts.

1.3.1. Experimental

Experimental studies that characterize thermal size effects will be classified in two groups. First group focuses on measuring the thermal conductivities of thin films and the second group directly measures the temperature of devices where localized heating is present. Experimental methods such as transient thermoreflectance techniques time domain thermoreflectance (TDTR), frequency domain thermoreflectance (FDTR), broad band frequency domain thermoreflectance (BB-FDTR); and then 3ω method are frequently employed to experimentally explore thin film conductivities, hence they are in the first group. Second group in the literature consists of methods such as optical spectroscopy and Micro-Raman spectroscopy and thermoreflectance imaging(TTI) which measures sample temperature [59–61].

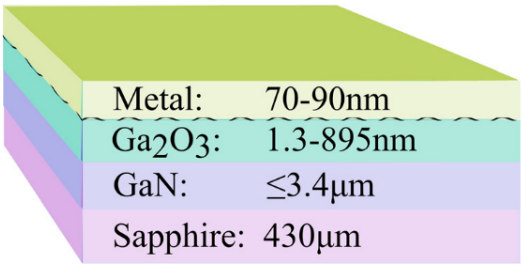

Figure 1.13. A TDTR sample schematic for $\beta - Ga_2O_3$ conductivity measurements of Szwejkowski *et al.* [58].

TDTR is based on detecting the changes in surface reflectance of thin films in response to heating. A laser is split into two branches: pump and the probe. Reflected probe beam from the material is compared to pump beam and the timing difference between two beams represent a tool to deduce thermal conductivity of the material [62]. FDTR form of this method is based on the frequency difference of these beams instead of the time delay [62]. On the other hand, BB-FDTR corresponds to the rearrangement of the conventional FDTR in order to cover higher modulation frequencies [62]. A common advantage of transient thermoreflectance methods is the ability of stacking thin layers of multiple thin films and performing measurements on them simultaneously as seen in Figure 1.13.

Invented by Cahill *et al.* in 1987 [63], 3ω method is another important experimental method which resides on detecting the voltage and resistance oscillations on a metal wire deposited on the sample. An alternating current is passed through the wire, causing harmonic temperature rises on both the wire and the sample [64].

Experimental options that measure sample temperature directly are frequently used to observe size effects. Such an example is Micro-Raman spectroscopy as visualized in Figure 1.14. Here, hotspot in an $AlGaN/GaN$ HEMT is targeted. Once temperature difference varying in hotspot is known, thermal conductivity in this confined area can be retrieved. In this method, excited photons are sent to the material and interfere with the vibrating molecules. A Raman spectrum is constructed. Raman signals (peaks) are tabulated as fingerprints for materials. Therefore, their shifts can be used to deduce the temperature difference and then the conductivity of the material. This method is frequently used for $AlGaN/GaN$ thermal characterization [61, 65–68].

To conclude, experimental attempts to measure thin film conductivities of WBG and UWBG materials are abundant. TTR, BB-FDTR and TDTR works performed on $AlGaN$ and $\beta - Ga_2O_3$ individually [58, 69, 70], and together [71] are present. On the other hand, these works are also performed for AlN and GaN, and they are occasionally accompanied by theoretical approaches [59, 72]. Moreover, instances of 3ω method conductivity measurements of both AlN and GaN are present in literature [23, 73–75].

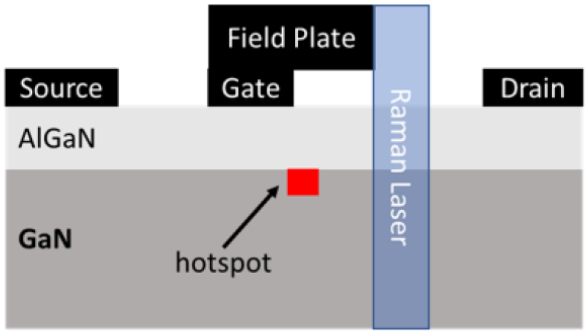

Figure 1.14. Micro-Raman spectroscopy measurement scheme of an $AlGaN/GaN$ device.

Experimental works in thermal conductivity and localized hotspot temperature characterization where thermal size effects are present are enlightening and they prove different thermal properties than that of bulk material. Yet, experimental set ups are expensive, and it goes without saying that experiments are also restricted with set up and measurement difficulties. For example, in thin films where quantum effects start to dominate, statistical uncertainties may be entailed [76] or Raman laser cannot pass through the field plate and yield an accurate thermal measurement of the hotspot which is underneath as seen in Figure 1.5. Thus, theoretical works are needed in order to foresee thermal size effects in micro/nanoscale devices for accurate thermal characterization. Theoretical works are expected to reduce the cost of the thermal conductivity estimations while also providing insight to thermal size effects without physical restrictions.

1.3.2. Theoretical

Theoretical studies that characterize thermal size effects will be classified in two groups. First group directly measures the temperature of devices where localized heating is present, and the second group focuses on measuring the thermal conductivities of thin films.

First group of the theoretical studies focuses on temperature profile of samples and devices. Frequently, approaches that solve Fourier Equation are used to complete this task [77]. Devices are modeled via finite element and/or finite volume analysis and temperature profile is predicted. However, in the presence of size effects, these approaches cannot be employed since materials' thermal conductivity is compromised. Then, phonon Boltzmann Transport Equation (BTE) should be addressed in order to model phonons and their contribution to bulk thermal conductivity [78].

Second group of theoretical studies, which focus on inherent material properties to model thermal conductivity is more successful in terms of addressing size effect problem. These studies include molecular and lattice dynamics, iterative solutions of BTE and ab-initio calculations [78, 79]. While molecular dynamics studies and iterative BTE solutions may tend to oversimplify materials' electronic structure, ab-initio (first-principle) calculations consider electronic properties when determining phonon properties. Moreover, most of the studies that calculate thermal conductivity do not offer an accumulation spectrum. For instance, Non-Equlibrium Molecular Dynamics (NEMD) simulations require a new run at each different length scale, this also results in enormous time consumption. Then the lost portion of the conductivity at continuous MFP scale stays unknown. This study uses an approach that meets these needs via combination of ab-initio calculations with thermal (phonon-based) calculations. As accumulation spectra will be obtained, each MFP length will have a corresponding conductivity contribution.

For UWBG materials, first principle works are present, and they tackle a diverse spectrum as well as thermal conductivity modeling [60, 80–83]. In literature, ab-initio calculations are frequently used for investigation of thin film thermal conductivity of materials. These investigations are not limited to thermal conductivity calculations: There are instances of first principles calculations utilized for mechanical properties such as elasticity, effect of doping and impurities on semiconductors [84], investigation of isotope ratio [56].

1.4. Phonon Thermal Conductivity - MFP Accumulation Spectra

Thermal accumulation spectrum, also noted as mean free path accumulation and thermal conductivity accumulation function in the literature, is the relation between accumulated thermal conductivity and the MFP of the material. To obtain this function is important in two aspects: Firstly, in the presence of size effects, it is impossible to predict the conductivity since it is not equal to bulk thermal conductivity. If the device in question is at nano or micro scale, it is extremely important to know how much of the bulk conductivity is covered by the sample. Then it will be possible to predict the thermal response of the device. Secondly, when the presence of size effects is unknown; accumulation spectrum is used. If the MFP range provided in the spectrum is crossed, one should expect to lose a portion of the bulk thermal conductivity. As seen in Figure 1.15, materials' thermal conductivity augments along the covered length until the coverage of total spectrum. Hence, accumulation spectrum is quite important in terms of expressing thermal behavior of micro and nano-scale samples. This section describes both experimental and theoretical attempts to build it.

In literature, one of the first detailed experimental accumulation spectra are obtained via Freedman *et al.* who built thermal conductivity accumulations of AlN, GaN, and other semiconductor materials as seen in Figure 1.15 [72]. Freedman *et al.* made use of TDTR method.

In Figure 1.9, it is visible that guidelines are drawn, in order to indicate how much of the bulk conductivity is preserved by the thin film at that MFP level. Beechem *et al.* also performed TDTR on GaN layers in order to define thermal conductivity accumulation [59]. Accumulation functions of both $AlGaN$ and β-form Ga_2O_3 are built via TDTR in literature as a function of device layer thickness [58, 69, 71].

Moreover, since most of the experiments include production of thin films of a certain size, to build a continuous accumulation function may present some difficulties and this may lead to a lack of data at the extremes of MFP spectrum.

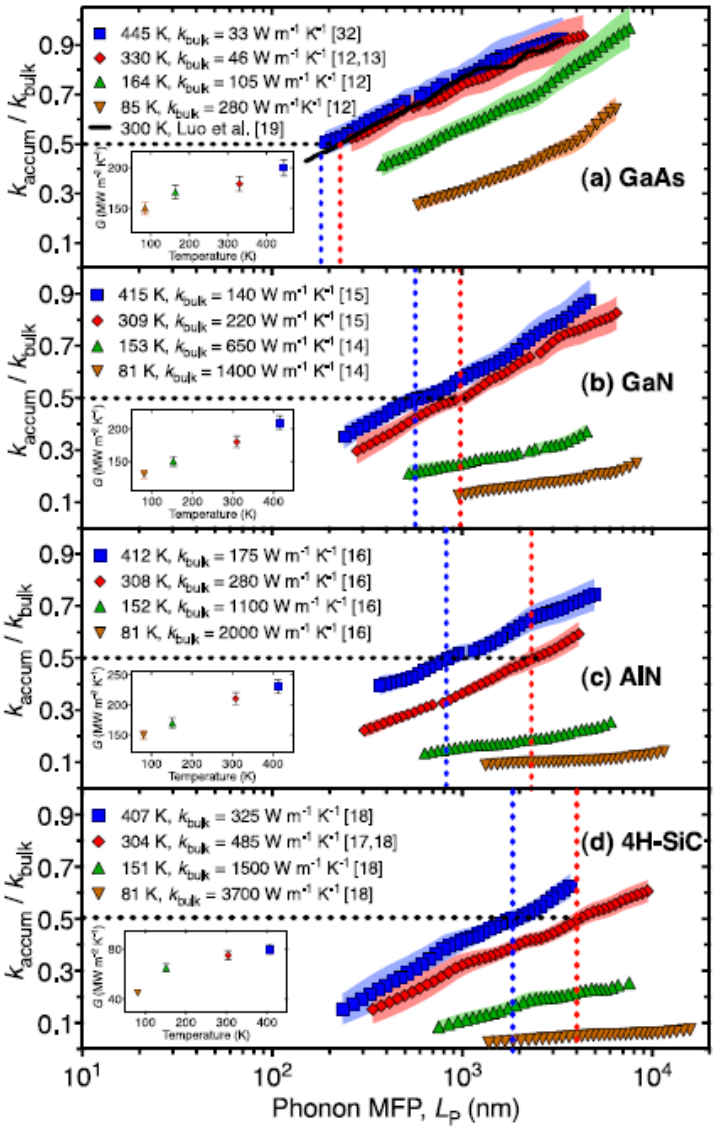

Figure 1.15. Thermal conductivity-MFP accumulation graphs obtained by Freedman *et al.* via TDTR [72].

There have been theoretical attempts to build thermal conductivity accumulation function. Most frequent way of tackling this problem is to perform first principles calculations and to incorporate them into phonon scattering rates with the usage of a phonon BTE solver such as ShengBTE or an in-house code [85]. This leads to calculation of phonon distribution to thermal conductivity, then accumulated conductivity assigned to each MFP value is known [86]. However, there are alternative approaches that use MFP as a free parameter and performs fitting with experimental values [87].

First-principles calculations provide phonon frequency data (i.e. phonon dispersion relation) and harmonic and anharmonic force constants are required to define crystal energy [88]. These constants are expected to yield a thorough understanding of phonon interactions via providing insight on the MFP that a phonon can travel and the relaxation time that a phonon has [89]. In most of these works, either iteration related methods such as Monte-Carlo simulations [90] or the harmonic approximation is employed. Harmonic approximation is an extension of spring analogy which suggests that atoms' movements can be modeled as masses connected with springs. Imaginary springs are modeled between atoms in order to understand the force that they exert to each other when lattice is perturbed (i.e. atoms are displaced).

Then, crystal ground energy (Φ) of the lattice is approximated as follows:

$$\begin{aligned}\Phi = \Phi_0 + \sum_{lk}\sum_{\alpha}\Phi_\alpha(lk)u_\alpha(lk) + \frac{1}{2}\sum_{ll'kk'}\sum_{\alpha\beta}\Phi_{\alpha\beta}(lk,l'k')u_\alpha(lk)u_\beta(l'k') \\ + \frac{1}{3!}\sum_{ll'l''kk'k''}\sum_{\alpha\beta\gamma}\Phi_{\alpha\beta\gamma}(lk,l'k',l''k'')\times u_\alpha(lk)u_\beta(l'k')u_\gamma(l''k'') + ...\end{aligned} \tag{1.3}$$

Here, as the spring analogy suggests, terms noted $\Phi_{\alpha\beta}$ refer to second order force constants (FC2) while $\Phi_{\alpha\beta\gamma}$ terms express third order force constants (FC3). α, β, and γ are Cartesian coordinates while $u(l,k)$ denotes displacement of atom number k in unit cell number l.

Harmonic approximation only considers second order force constants (FC2s) (which can be observed in Equation 1.3) obtained via phonon dispersion relation and tackles the rest with approximations. Phonon interactions are frequently modeled using Grüneisen parameter or via fitting the bulk conductivity to previously tabulated conductivity value. Depending heavily on approximations and fitting parameters might be a danger since these parameters are dependent on individual samples. Then these studies cannot be generalized and used in all predictions. As it will be further explained in the following sections, the aim and novelty of this work is to include third order force constants (FC3s) for all of the four materials, which are the coefficients that appear

as crystal ground energy approximation is further expanded as seen in Equation 1.3. As FC3s are included in thermal conductivity calculations, it is expected to obtain accurate thermal conductivity results without resorting to approximations [91].

Finally, theoretical accumulation spectrum works are relatively abundant for GaN since it is a popularly used material [56, 82, 90, 92, 93]. On the other hand, theoretical MFP calculations combined with first principles are rather rarely focused on AlN, $AlGaN$, and $\beta - Ga_2O_3$ [87, 94–97].

1.5. Motivation & Problem Definition

As it is explored in previous sections, UWBG materials GaN, AlN, $AlGaN$ and $\beta - Ga_2O_3$ are frequently employed in high power electronic devices. These materials, often in thin film or other small scale forms such as nanowires or hotspots, can have localized heating which may result in non-continuum thermal transport behavior. This behavior can cause devices to heat unexpectedly, hence degradation due to excessive heating follows. Shorter device lifetime represents a waste of both material and energy, leading to economic and environmental drawbacks.

The reason underlying the thermal transport deviation from continuum behavior is related to MFP of thermally conductive phonons. Phonon MFP, which is the path that a phonon can travel before facing a collision, reigns thermal conductivity. In non-continuum thermal transport phonons are interrupted before they complete their MFP length journey and fail to conduct thermal energy diffusively.

As it was mentioned in previous sections, accumulation spectrum helps prediction of thermal conductivity of confined structures where size effects are in play. Since phonon MFP thermal conductivity accumulation spectra displays the relationship of MFP and thermal conductivity, it allows to predict thermal conductivity value at a certain length scale. Thus, it is necessary to obtain accumulation spectra to address the size effect issues.

Experimental attempts to obtain accumulation spectra requires a considerable amount of time and effort. When the fact that experimental set ups and samples are costly is added, it is obvious that an accurate theoretical approach is needed. On the other hand, most of the theoretical methods rely heavily on approximations and fitting parameters. Some other theoretical approaches such as molecular dynamics simulations require the calculations to be repeated at each length scale, hence they fail to provide a continuous accumulation spectrum and are time consuming.

The main motive of this thesis is to obtain phonon accumulation spectra of four WBG and UWBG materials GaN, AlN, $AlGaN$, and $\beta - Ga_2O_3$ via ab-initio calculations and employment of third order force constants. It is attempted to construct MFP-thermal conductivity accumulation of mentioned materials while avoiding the cost and errors of experimental setups. Finally, it is also aimed to obtain guidelines on how to use these accumulation spectra to obtain thermal conductivity of confined structures. A method is presented to retrieve small scale conductivity from accumulation spectrum. Accumulation spectra will help to enhance device lifetime by predicting devices' thermal responses at small scales.

1.6. Outline of Thesis

Following sections of this thesis have the final aim of constructing accumulation spectra of AlN, GaN, $AlGaN$, and $\beta - Ga_2O_3$. In order to achieve that, ab-initio calculations and thermal calculations are carried out via VASP and Phono3py software, respectively. Second chapter following the introduction will provide an insight on methodology of this thesis. Introduction provided definitions of basic notions related to this study such as phonon, MFP, and relaxation time. Then Chapter 2 will provide necessary equations accompanied by logical flow of used software with additional definitions such as force constants and phonon group velocity.

Then, Chapter 3 will include results of this study. Accumulated thermal conductivity spectra will be provided for four materials. Accumulation spectrum, as well as reached bulk thermal conductivity results of materials will be provided at different

temperatures. Chapter 3 will also include comparison of results with literature. Accumulation of all four materials will be compared with results from both experimental and theoretical studies in literature. Accumulation results will also be compared with each other in order to discuss materials' difference in terms of accumulation spectrum. Then, deviations from each other and literature will be discussed at the end of Chapter 3.

Chapter 4 will provide thin film and confined space applications of this work's findings. Since thermal conductivity accumulation spectra is provided in previous chapter, it is now possible to apply these to literature examples. Most popular confined structures in the industry are thin film forms for all four of the materials. Accumulation spectra provides an idea of how much of the conductivity is preserved at a certain length scale, hence thin film conductivity deductions are made. Then, both experimental and theoretical instances of thin film conductivities in literature are used for comparison.

Chapter 5 will be focused on conclusion and implications of this work. Deductions stemming from Chapters 3 and 4 will be discussed. The effect of using third order force constants on thermal accumulation- MFP spectrum will be examined while also considering anharmonicity in materials. Interpretation of accumulation spectrum in terms of thin film thickness will be carried out. Finally, future work possibilities that can be performed in the light of this study will be explored as the conclusion of this study.

2. METHOD

This study attempts to obtain thermal conductivities and accumulation spectra of four materials: GaN, AlN, $AlGaN$ and $\beta - Ga_2O_3$. In order to realize these aims, ab-initio and thermal calculations are employed. This section is to describe the theoretical path of this process.

As Figure 2.1 shows, calculations of this work are completed via two software: Vienna Ab-initio Simulation Package (VASP) and Phono3py. Firstly, unit cells of materials are processed via VASP: ionic, then geometric relaxation is performed in order to have proper initial conditions. Relaxed unit cell is fed to Phono3py and is multiplied to ensure replication of unit cell. This multiplied structure is called supercell. Then, a small displacement is introduced to supercell structure. Displacements are kept in different folders and self-consistent field (SCF) calculations are performed on each displacement. Then, all folders are scanned by Phono3py and forces acting on the structure is processed in the light of displacement values. This process provides second and third order force constants.

Then, these constants are incorporated into dynamical matrix in Phono3py and employed in calculating both phonon dispersion and inverse relaxation times. These data are used to find all phonon properties such as group velocity, MFP and finally; accumulated thermal conductivity.

2.1. Ab-initio Calculations

Ab-initio calculations of this work is performed via Vienna Ab-Initio Simulation Package (VASP), which is a software initiated by Mike Payne [98]. After the initiation, the code is further developed in University of Vienna and took its current shape. VASP is an ab-initio calculator for atomic scale modeling that adopts either the project augmented wave (PAW) method with a plane wave basis set or the pseudopotential approach [99–102]. Pseudopotentials assume that core electrons are not affected by the

electronic state of the atom, therefore they are used to approximate the many body Schrödinger equation. A simple form of Schrödinger Equation is visible in Equation 2.1. In Equation 2.1, $\hbar$ denotes reduced Plank constant.

$$-\frac{\hbar^2}{2m}\nabla^2\psi_t + U\psi_t = i\hbar\frac{\partial\psi_t}{\partial t} \tag{2.1}$$

As seen in Equation 2.1, Schrödinger Equation relates wave function ψ_t which encapsulates the position of an electron or a photon, with the energy U. When more bodies are considered, Schrödinger Equation takes an even more complex form. Hohenberg and Kohn tackled this problem in a creative way: they postulated two assumptions: Energy can be expressed as a function of energy density and the ground state energy can be determined [98]. This represent the basis of Density Functional Theory (DFT) method which states that multiple body problems can be solved via the usage of functionals (a functional is the function of a function) of electron density depending on a single position variable. This paved the way for iterations in VASP scheme seen

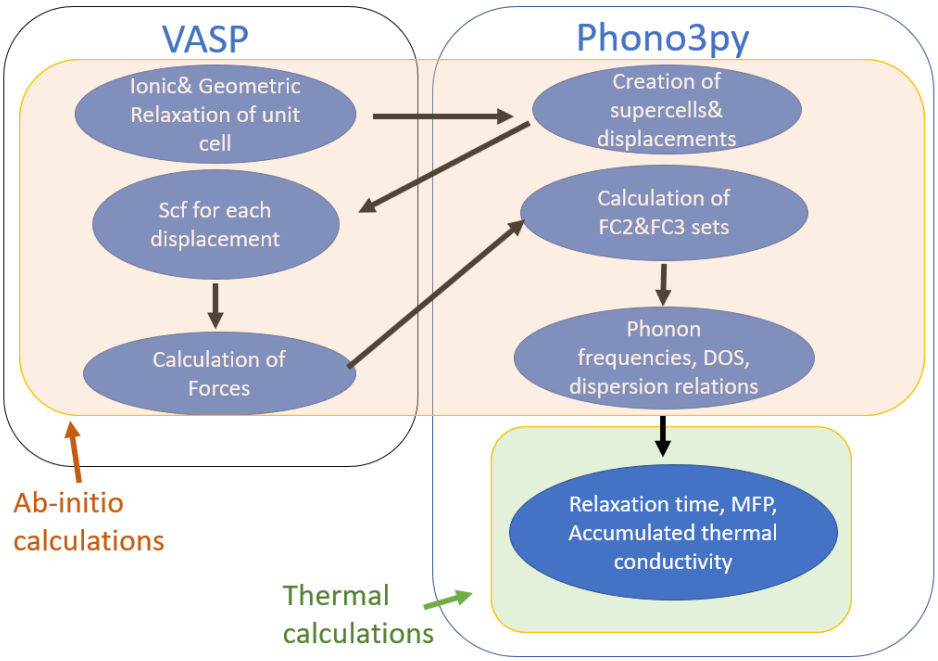

Figure 2.1. Overall workflow of calculations.

in Figure 1.11. Moreover, Kohn Sham equations were formed as seen in Equation 2.2. These equations formulate single-electron wavefunctions and express them to depend only on spatial variable r, as it is suggested by DFT scheme. Here in Equation 2.2, $V(r)$ denotes the defined part of the energy functional. This potential defines the interaction between an electron and the total of atomic nuclei. $V_H(r)$ is Hartree potential and $V_{xc}(r)$ is the functional derivative of exchange-correlation energy.

$$\left[-\frac{\hbar^2}{2m}\nabla^2 + V(r) + V_H(r) + V_{xc}(r) \right] \psi(r) = \epsilon_i \psi(r) \tag{2.2}$$

VASP operates with self-consistency scheme to solve Kohn-Sham equations which are crucial to define the wave functions. This implies that the program iterates density functions to check the convergence of the wavesets as shown in Figure 2.2. It can be stated that VASP uses the free energy as a parameter and attempts to define the electronic ground state. As seen Figure 2.2, this solution process helps defining the force constants for this study.

VASP operation is based on four main input files which hold information of both material and calculation process. First input file is called INCAR, which describes the calculation process. INCAR tells VASP which calculation to perform as well as parallel processing details such as number of cores to occupy while functioning. Second input file is called POTCAR which includes electronic potentials of the elements involved in the calculation. Third input file, POSCAR, preserves crystallographic information such as the types and positions of the atoms. Final input file that is needed is called KPOINTS, which helps the user define number and sort of the meshes for the calculation [98].While results of the calculations are distributed to files such as OUTCAR, it is preferred to retrieve data from VASP directly via *vasp.xml* folders. The force constant matrices of second and third order are the main outcome of ab-initio calculations. These results are stored in displacement folders. Displacement folders are later retrieved and used in another software, Phono3py. Developed by Togo *et al.*, Phono3py inherits force constants and employs them in defining phonon properties [86, 88, 89]. First operation

of Phono3py is to inherit the unit cell from VASP that is ionically and geometrically relaxed. Phono3py replicates this unit cell in user specified dimensions (e.g. $3 \times 3 \times 2$) and creates a supercell as seen in Figure 2.3. Then a displacement is introduced to this supercell and the reaction of the cell is stored under different displacement folders. These folders are than scanned by VASP in order to perform scf calculations. Output data of these scf calculations are processed by Phono3py once more. Since crystal energy is approximated as seen in Equation 1.3, Phono3py makes use of displacements

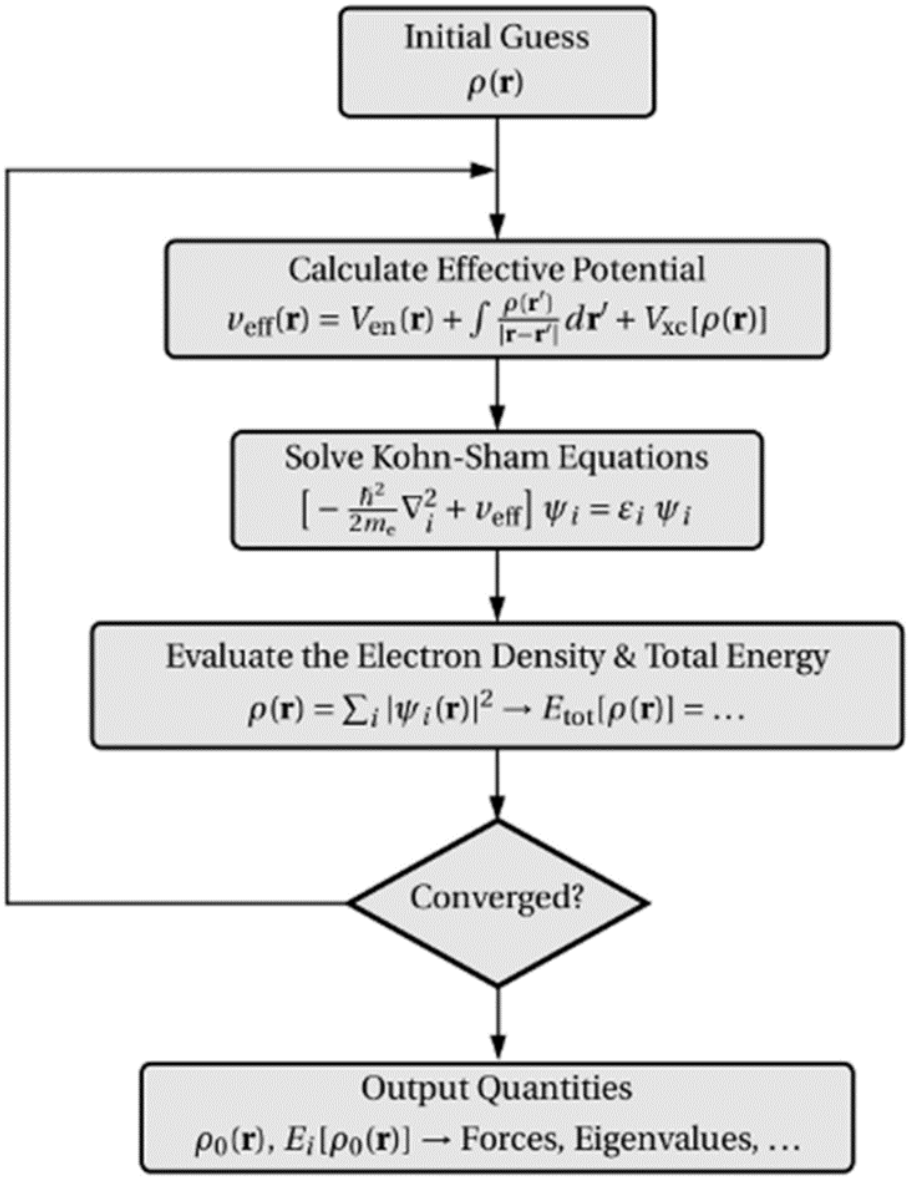

Figure 2.2. Self-Consistent Field (SCF) Scheme of VASP.

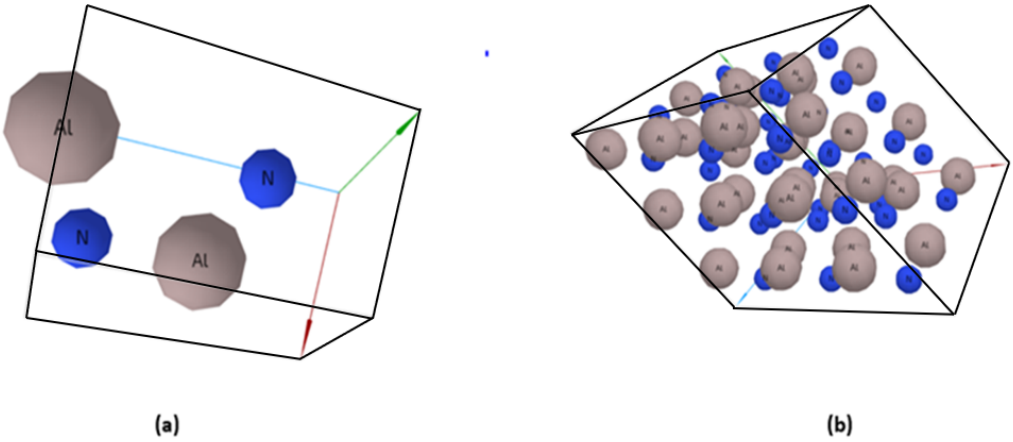

Figure 2.3. Schematic displaying (a) Unit cell, (b) Supercell structure of AlN.

and takes the derivative of the energy with respect to displacements to retrieve FC2 and FC3 sets.Then, these sets are employed in thermal calculations.

2.2. Thermal Calculations

Thermal calculations are performed using phonon dispersion data and second and third order force constants via Phono3py. To obtain accumulated conductivity, one needs to refer to Equation 2.3. Here, k is the bulk thermal conductivity and the other terms are as follows: N is the number of unit cells in the sample, V_0 is the volume of the unit cell, c_{qs} is specific heat, v_{qs} is group velocity and τ_{qs} is the relaxation time.

$$k = \sum k_{qs} = \frac{1}{NV_0} \sum c_{qs} v_{qs} \otimes v_{qs} \tau_{qs} \tag{2.3}$$

Specific heat is a direct function of phonon frequency ω_{qs} and temperature T as seen in Equation 2.4. Here in Equation 2.4, k_b is Boltzmann constant.

$$c_{qs} = \frac{k_b \left(\frac{\hbar\omega_{qs}}{k_b T}\right)^2 \exp\left(\frac{\hbar\omega_{qs}}{k_b T}\right)}{\left[\left(\frac{\hbar\omega_{qs}}{k_b T}\right) - 1\right]^2} \tag{2.4}$$

On the other hand, group velocity is defined as in Equation 2.5. It is directly related to phonon dispersion equation since it is the derivation of dispersion with respect to wavevector q as seen in Equation 2.5.

$$v_{qs} = \frac{\partial \omega_{qs}}{\partial q} \tag{2.5}$$

FC3, i.e. third order force constants are incorporated into relaxation time approximations. As seen in Equation 2.6, these force constants are directly converted via dynamical matrix into $\Phi_{-qsq's'q''s''}$ term which describes phonon interaction rates of modes qs, $q's'$ and $q''s''$, hence, they have a direct effect on inverse relaxation time [86, 89]. Here in Equation 2.6, $n_{q's'}$ denotes the phonon equilibrium occupation number which is calculated through Equation 2.7.

$$\begin{aligned}\Gamma_{qs} =& \frac{18\pi}{\hbar^2} \sum_{q's'q''s''} \left|\Phi_{-qsq's'q''s''}\right|^2 \big\{(n_{q's'} + n_{q''s''} + 1)\delta(\omega - \omega_{q's'} - \omega_{q''s''}) \\ &+ (n_{q's'} - n_{q''s''})\big[\delta(\omega + \omega_{q's'} - \omega_{q''s''}) - \delta(\omega - \omega_{q's'} - \omega_{q''s''})\big]\big\}\end{aligned} \tag{2.6}$$

$$n_{qs} = \frac{1}{\exp\left(\dfrac{\hbar\omega_{qs}}{k_B T}\right) - 1} \tag{2.7}$$

Then, inverse phonon lifetime Γ_{qs} is simply converted to phonon lifetime τ_{qs} via Equation 2.8.

$$\tau_{qs} = \frac{1}{2\Gamma_{qs}(\omega_{qs})} \tag{2.8}$$

Since phonon MFP Λ_{qs} is dependent on phonon lifetime and group velocity as seen in Equation 2.9, now all findings can be plugged into conductivity calculation described in Equation 2.3.

$$\Lambda_{qs} = \tau_{qs} v_{qs} \tag{2.9}$$

Then, since contribution of each phonon mode qs is defined, they can be summed as in Equation 2.10 to explain conductivity accumulation in terms of MFP Λ. Finally, thermal conductivity can be expressed in the form of accumulation function.

$$k_{acc}(\Lambda) = \sum_{\Lambda_{qs}=0}^{\Lambda_{qs}=\Lambda} k_{qs} \tag{2.10}$$

3. RESULTS

3.1. *GaN*

As it is the case for multiple Group III-V nitride materials, GaN is usually found in wurtzite or zinc-blende(cubic) configuration [103]. Hence this work is realized on wurtzite form of GaN. GaN lattice parameters are accepted as $a = 3.18$ $\mathring{A}$ and $c = 5.19$ $\mathring{A}$ [103]. Unit cell of GaN which consists of four atoms is replicated in order to obtain a $3\times3\times2$ supercell for third-order FC calculations. To have more accurate results, second order FC calculations are obtained via larger supercell which has dimensions of $5\times5\times3$. Due to time restrictions of calculations, a cut-off distance of 3.17 $\mathring{A}$ was applied to the system. The cut-off distance defines the distance beyond which phonon interactions are ignored. Cut-off distance reduced the number of displacements remarkably. Thermal calculations are performed using a $24 \times 24 \times 24$ mesh.

Phonon dispersion results of wurtzite GaN are visualized via Phonopy as seen in Figure 3.1. Bandgap of GaN was reached as 5.6 THz and is in accordance with Broido *et al.*'s work [56]. Phonon branches are plotted along Brillouin zone which was described in Figure 1.11.

Bulk conductivity results of GaN are found as follows: 225.6 W/m-K, 138.88 W/m-K, and 87.34 W/m-K at 300 K, 500 K and 800 K, respectively. Bulk conductivity at 300 K for wurtzite GaN is reported as 220 W/m-K by Freedman *et al.* [72], 227 W/m-K by Slack *et al.* [104] and 226 W/m-K by Jezowski *et al.* [105]. Thus, 225.6 W/m-K at 300 K is in good agreement with literature.

Accumulation spectra of GaN at 300 K, 500 K, and 800 K are given in Figure 3.2. As in Figure 3.2 half of the conductivity is contributed by phonons with MFPs smaller than 260 nm at 300 K. MFP of thermally conductive phonons reaches to 1661.7 nm at 300 K. Some critical MFP values in terms of contribution is visible in Table 3.1. As temperature rises, MFP spectrum shortens as a result of increased phonon scattering.

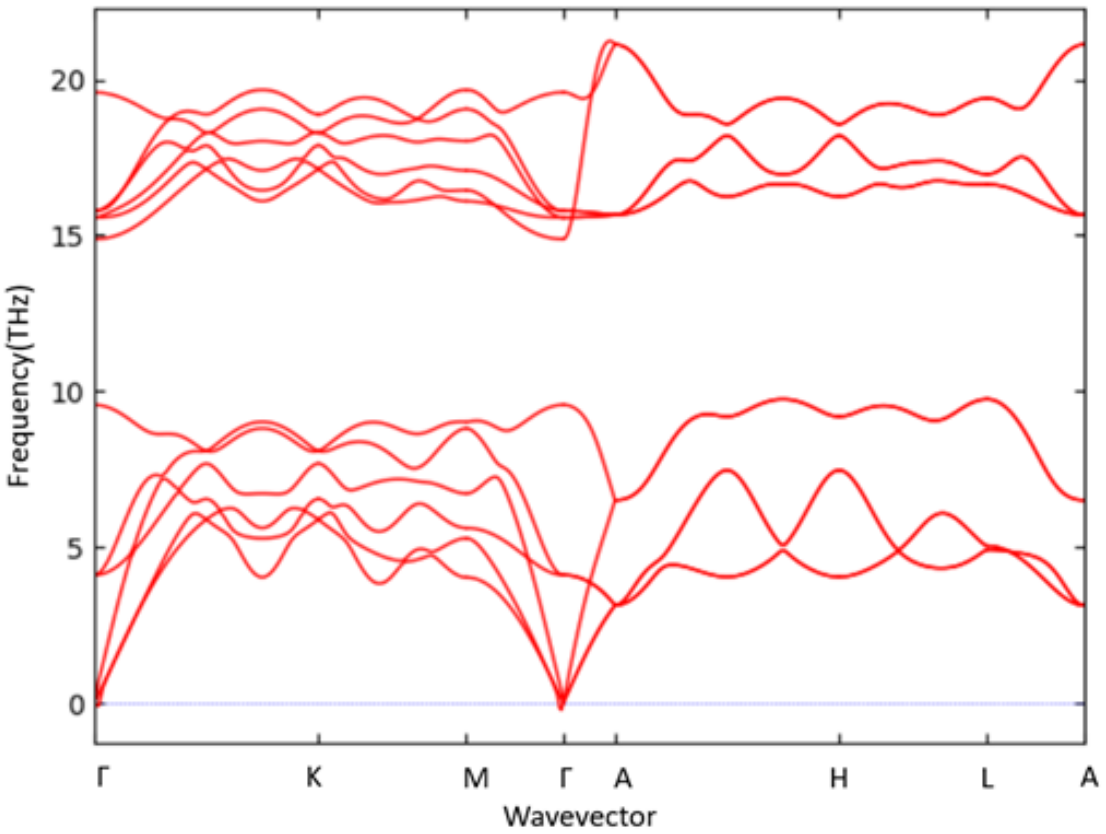

Figure 3.1. Phonon dispersion curve of GaN.

Results obtained in this study is compared with the accumulation spectra from literature in Figure 3.3. Here, theoretical work of Hu *et al.* and TDTR results of both Freedman *et al.* and Beechem *et al.* are employed [59,60,72]. The accumulation spectra presented in this study spans a shorter phonon MFP spectrum than the experimentally

Table 3.1. MFP of phonons contributing to 30%, 50%, and 90% of the bulk wurtzite GaN thermal conductivity (k) at various temperatures.

Temperature (Kelvin)	**30% of k**	**50% of k**	**90% of k**	**Total (100%) of k**
300	>168 nm	>262 nm	>589 nm	<1661.7 nm
500	>94 nm	>147 nm	>322 nm	<562.2 nm
800	>58 nm	>89 nm	>195 nm	<344 nm

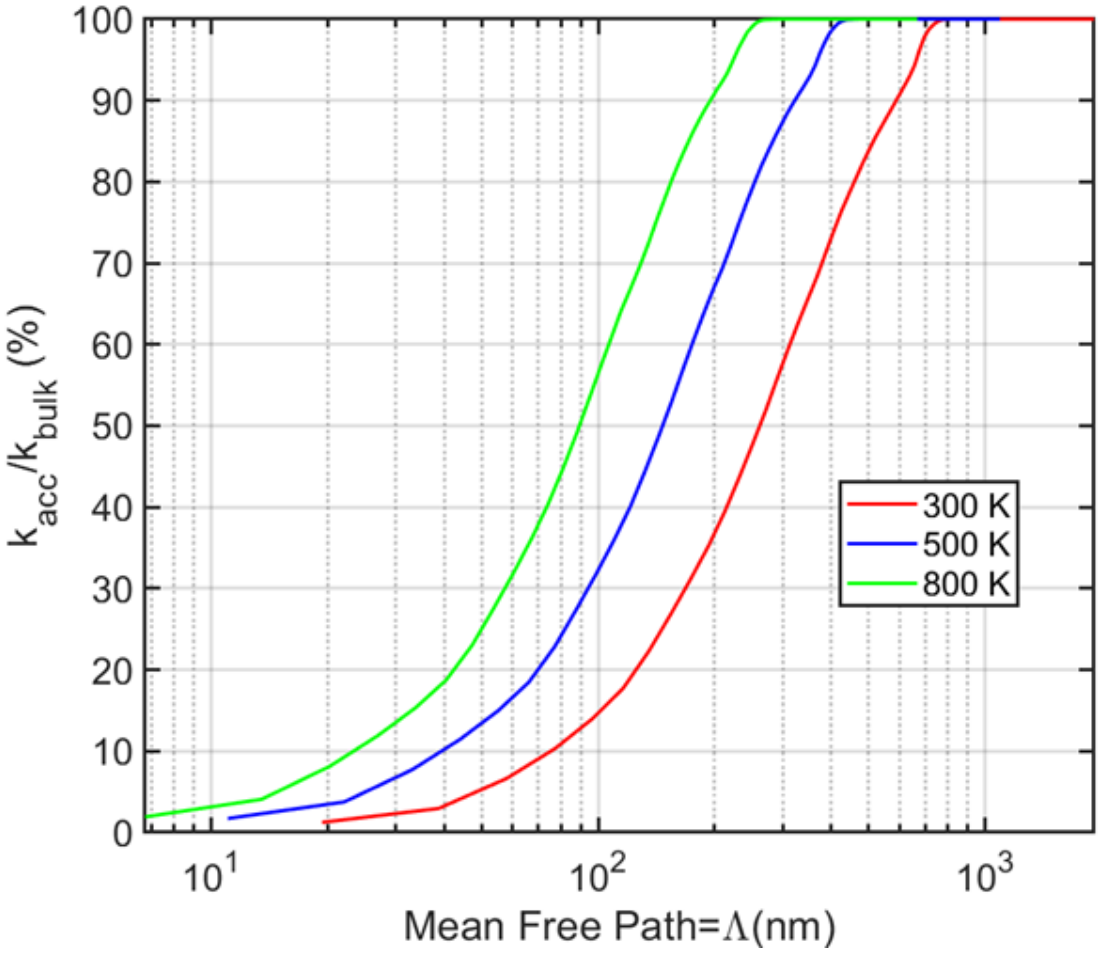

Figure 3.2. Accumulation spectra of *GaN* at 300 K, 500 K and 800 K.

obtained spectra in literature. Yet, theoretically obtained accumulation spectra of Hu *et al*. also spans a shorter MFP spectrum and agrees better with this work [60]. The discrepancy between experimental and theoretical samples may stem from the quality of the samples and/or resolution and uncertainties of the experiments. Theoretical studies in general assume a perfect lattice, free of dislocations and impurities. Yet experimental samples naturally have these problems. Moreover, TDTR method, employed by Beechem *et al*. and Freedman *et al*., may entail statistical errors [76]. Besides statistical errors,several other problems of both TDTR and FDTR experiments are reported [62]. Multiple unknown properties such as heat capacity are approximated, and multiple fitting parameters are used in TDTR and FDTR [62]. Number of these fitting parameters may be up to 48 [106].Moreover,uncertainties related to experimental set

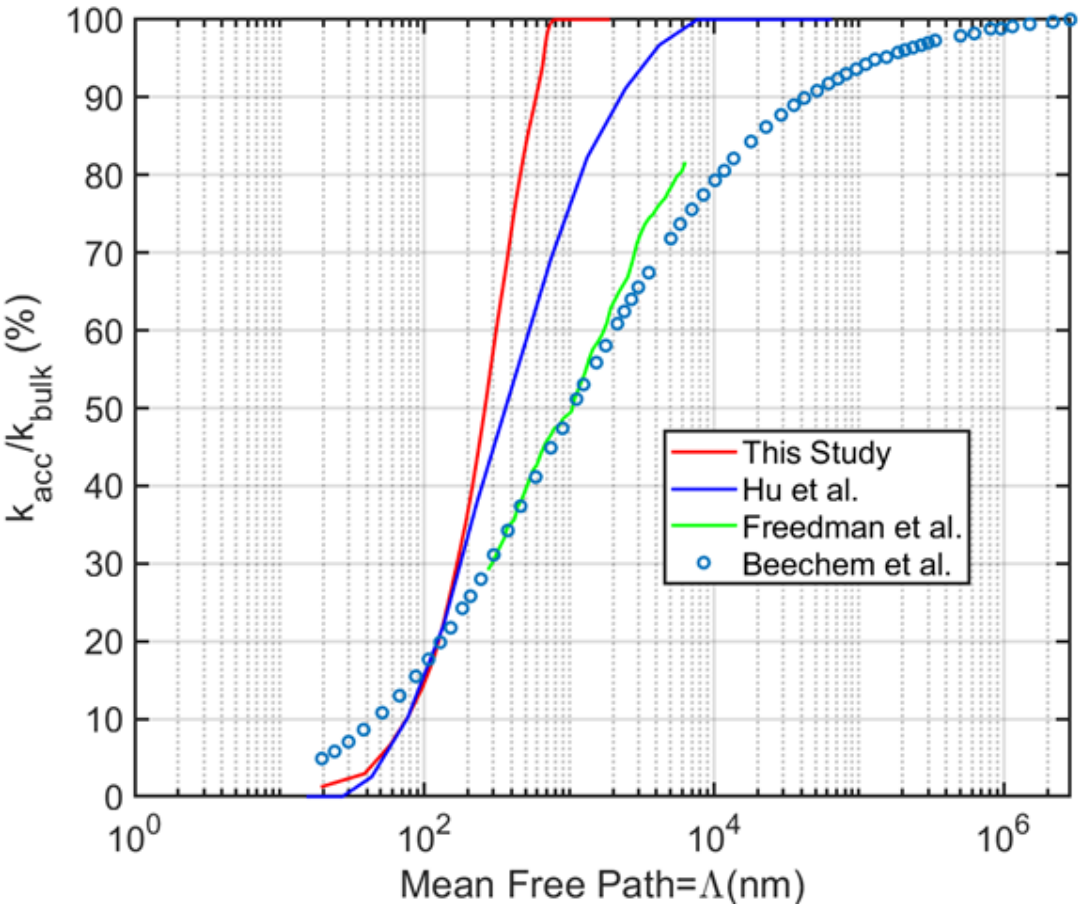

Figure 3.3. Comparison of this study with literature.

ups are several: large laser spot may decrease resolution, self heating may interfere with the results and small penetration depth may cause erroneous findings [62]. Thus, it is visible that experimental results are expected to deviate from theoretical models.

These results are also compared with the results obtained using a harmonic approximation with the usage of third order FCs [91]. As it was explained in the previous sections, harmonic approximation uses a fitting parameter. The harmonic approximation used in Figure 3.4 considers only second order FC set, hence it operates only on phonon dispersion data. This approximation can be used to explain experimental findings and yields closer MFP spectra to experimental works. Nevertheless, in this method, thermal conductivity is fitted to a predetermined value, then other parameters such as MFP, phonon scattering rate and relaxation time are also subjected to fitting.

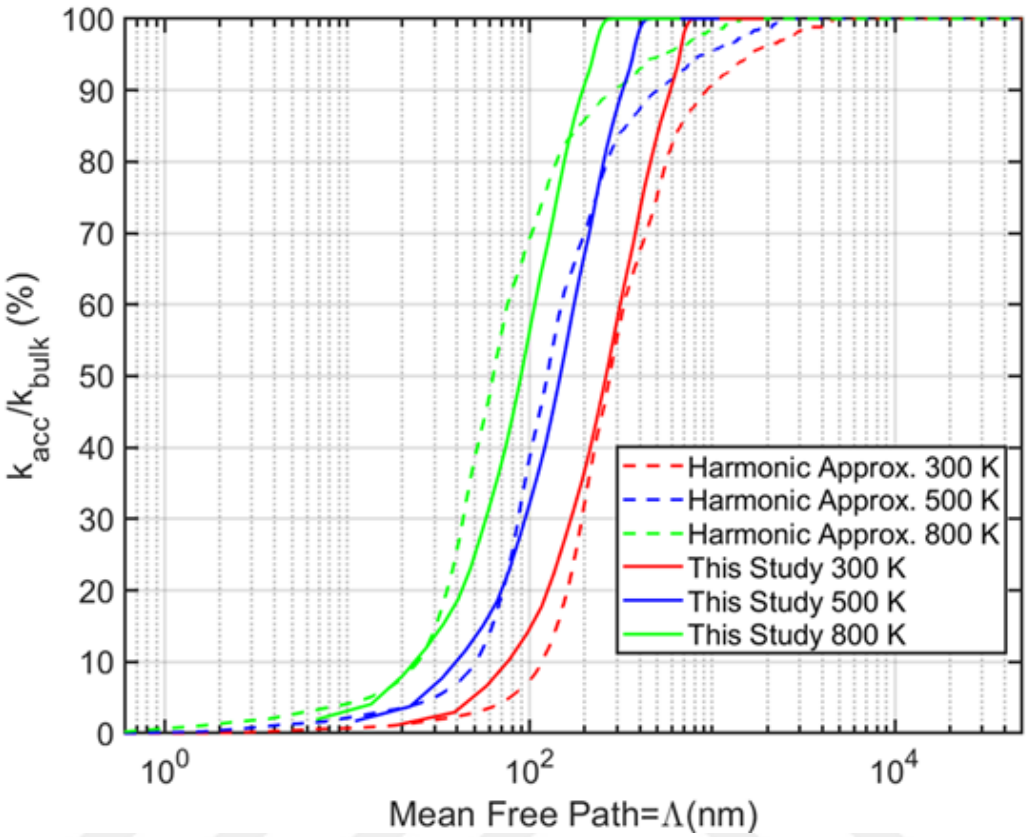

Figure 3.4. Comparison of this study with harmonic approximation [91]

Therefore, it can be stated that harmonic approach is heavily dependent on fitting data. This dependence makes it difficult to generalize its findings: an example with a different thermal conductivity will generate a different accumulation spectrum.

As temperature increases, harmonic approximation and the method presented in this thesis yield similar spectra. Yet at high temperatures and shorter length scales phonon-phonon interaction increases and anharmonicity becomes important. Thus, using third order FCs result in more accurate depiction of crystal ground energy (since it includes further terms in approximation given in Equation 1.3), and provide more accurate results where anharmonicity exists.

Finally, obtained GaN results are compared with experimental and theoretical findings in literature. GaN spectra of this work were also compared to a theoretical

method which uses harmonic approach. It was found that using third order FCs yields accurate bulk thermal conductivities. On the other hand, calculated MFP spectra were shorter at low temperature. It was concluded that in cases where anharmonicity is increased (localized heating, high temperature), using third order FCs yields accurate MFP results without approximation.

3.2. AlN

As a non-oxide ceramic, aluminum nitride is a Group III-V nitride material. While it can have multiple lattice structures which are cubic (rock salt and zinc-blend) [107], this study examines its wurtzite form which is a hexagonal closed packed (HCP) form, noted as $h-AlN$ [108]. This preference has its roots in cubic forms being metastable phases, i.e. they tend to change to a more stable form during different manufacturing processes. As a result of this lack of stability, AlN structures are usually produced from $h-AlN$. Hence, it is reasonable to choose this closed pack form for a thin film study.

Calculation process of AlN is quite similar to GaN. Both structures have unit cells of four atoms. As it was also the case for GaN, a $3\times3\times2$ supercell was employed for third order force constants calculations and a $5\times5\times3$ supercell was chosen for second order force calculations for AlN. A cut off distance of 3.0 $\mathring{A}$ was employed to reduce the number of calculations steps. Thermal calculations are performed via $38\times38\times24$ mesh. Phonon dispersion relation of AlN is plotted as seen in Figure 3.5 and agrees with literature [81].

Phonon frequencies and force constants sets were imported and processed in order to obtain thermal properties. Bulk thermal conductivity values of AlN were calculated as 199.3 W/m-K , 136.2 W/m-K, 104.4 W/m-K and 85.12 W/m-K at 300 K, 400 K, 500 K and 600 K respectively. At 300 K, AlN bulk thermal conductivity resides in the interval of 170-220 W/m-K as reported by Júnior *et al.* [26].

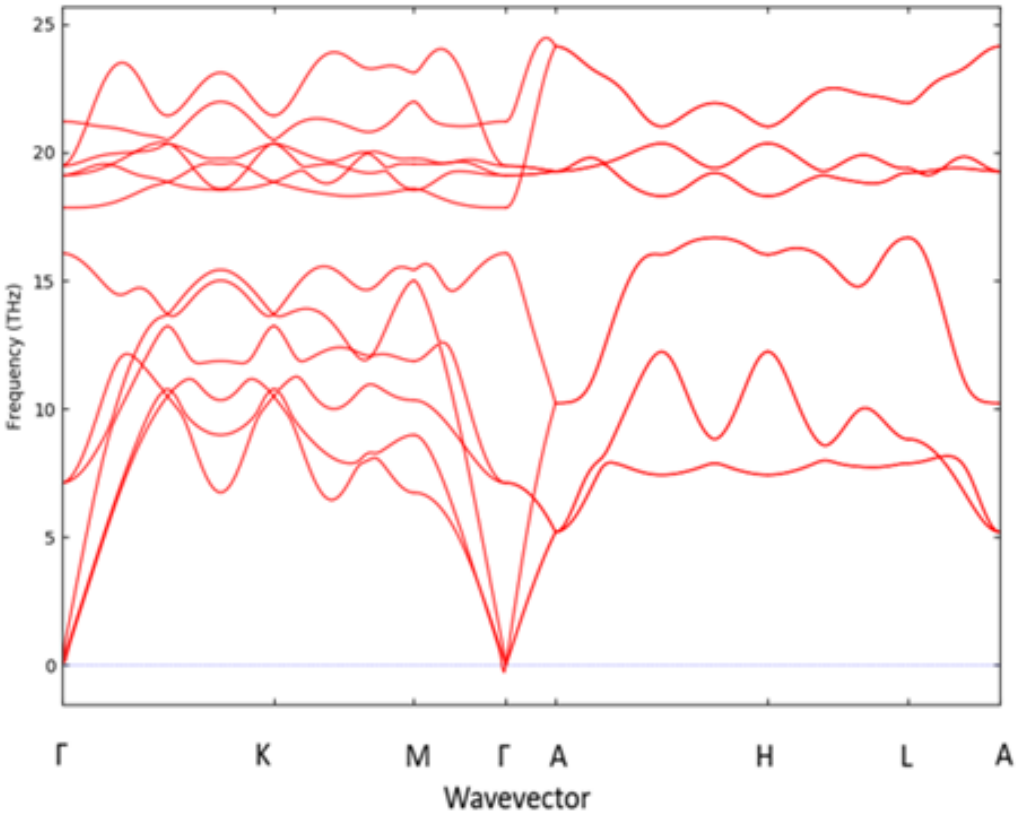

Figure 3.5. Phonon dispersion relation of AlN.

Found accumulation spectra are shown as seen in Figure 3.6. Accumulation spectra are also calculated at 300 K, 400 K ,500 K and 600 K. MFP values of thermally active phonons at different conductivity proportions are shown in Table 3.2. As expected, spectrum gets shorter with the increasing temperature. This implies that as heating is increased in device, size effects are expected to appear at smaller scales and further phonon entrapment is expected.

Accumulation spectra at 300 K and 400 K are compared to examples in literature. Previous studies of AlN is limited compared to GaN. Freedman *et al.*'s TDTR work at close temperatures was used for comparison [72]. Similar to GaN, wurtzite AlN spectra are shorter than experimental results. However, it is visible in Figure 3.7 that as temperature rises, resulting spectrum gets closer to experimental values. This once

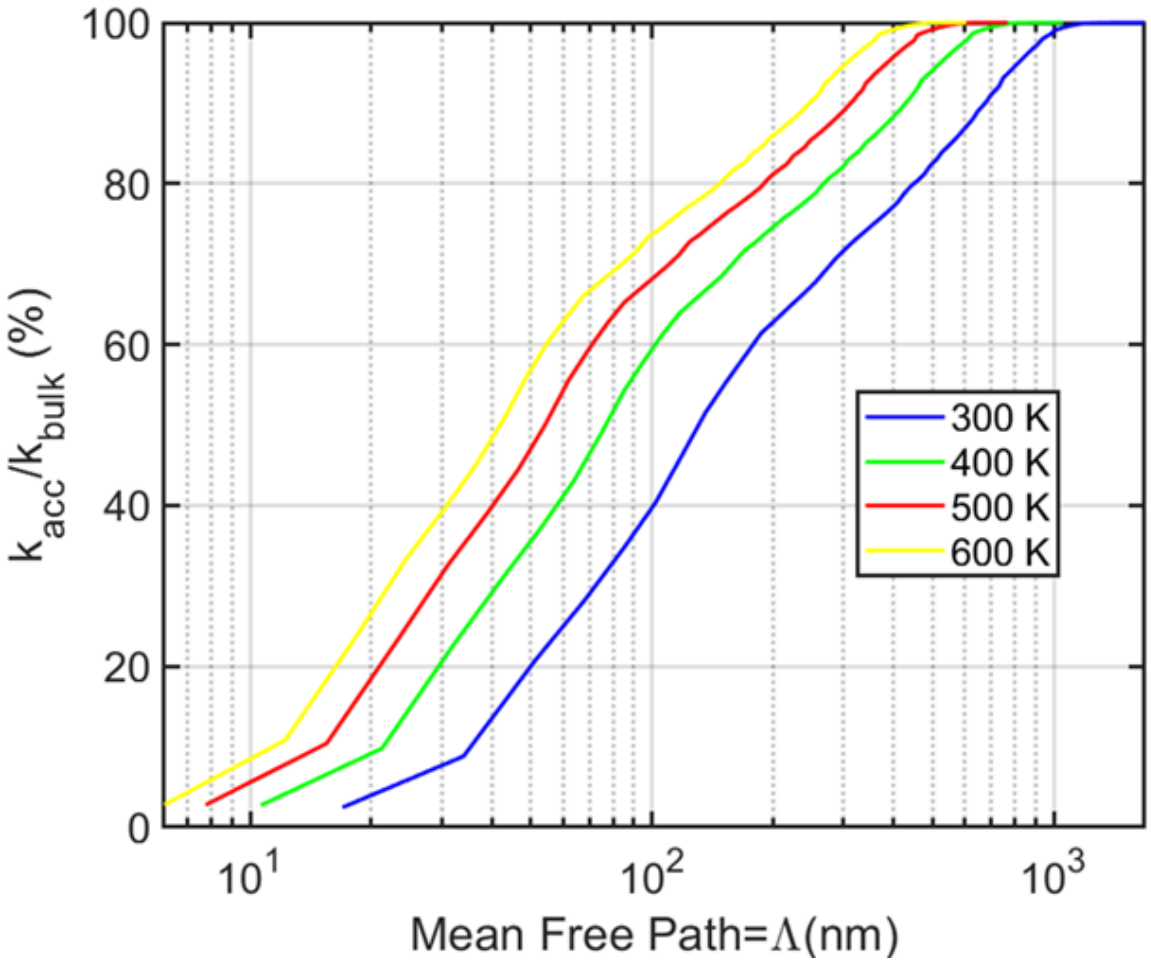

Figure 3.6. Accumulation spectra of AlN at 300 K, 400 K, 500 K and 600 K.

Table 3.2. MFP of phonons contributing to 30%, 50%, and 90% of bulk wurtzite AlN thermal conductivity (k) at various temperatures.

Temperature (Kelvin)	**30% of k**	**50% of k**	**90% of k**	**Total (100%) of k**
300	>72.4 nm	>131 nm	>674 nm	<1648.8 nm
400	>41 nm	>77 nm	>428 nm	<1033 nm
500	>28.7 nm	>54 nm	>312 nm	<759 nm
600	>22 nm	>42 nm	>247 nm	<593 nm

again demonstrates that third order FC helps to cover anharmonicity. Moreover, a more recent work which was performed by Park and Kim [109] was also included in order to validate accumulation spectra. Park and Kim experimented on RF (radio frequency) magnetron sputtered thin film samples having the thickness of 200 nm. They report 50% of AlN bulk conductivity at this scale, which is closer to this study than Freedman *et al.*'s work. Several uncertainties of FDTR method were already discussed, then there is a possibility of FDTR to overestimate MFP spectrum due to both experimental restrictions and multiple approximations [62].

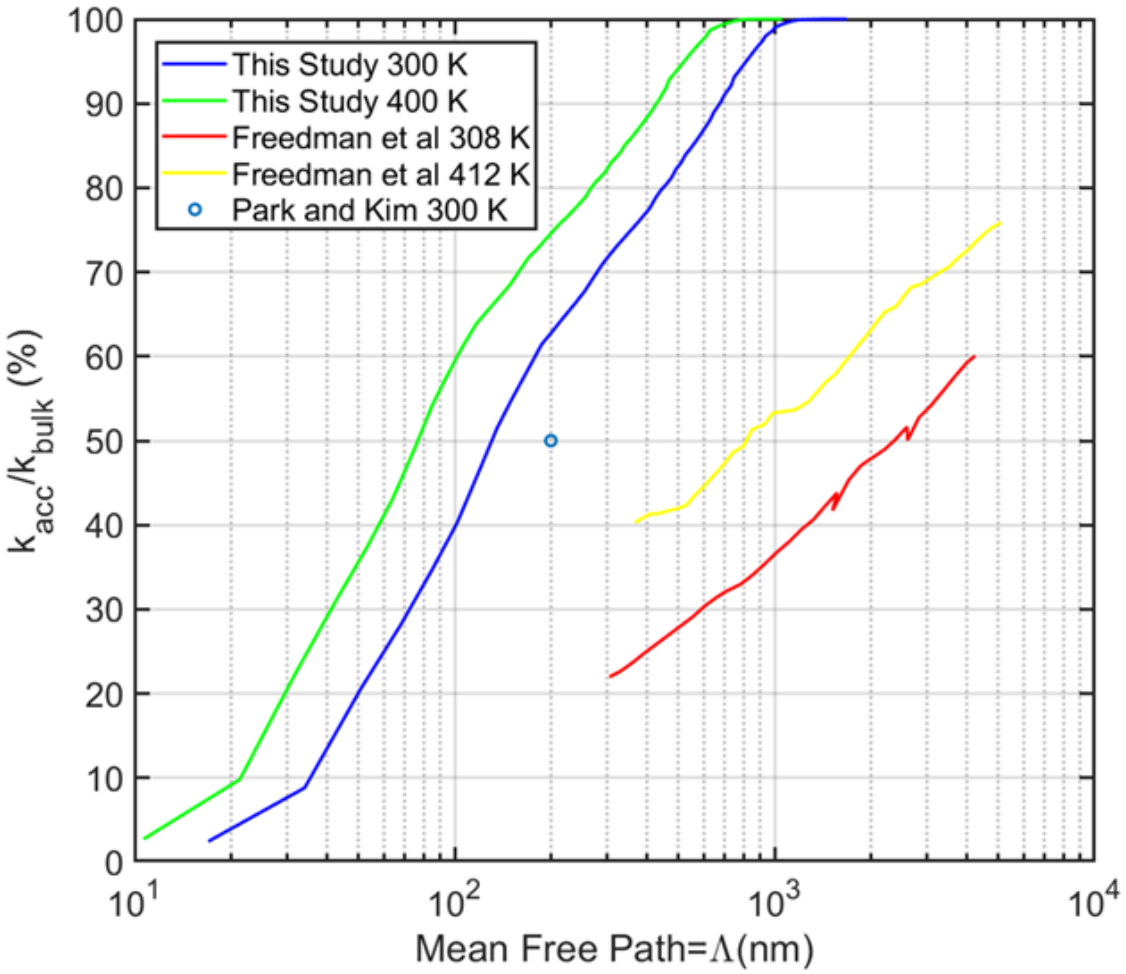

Figure 3.7. Literature comparison of AlN at with works of Freedman *et al.* and Park *et al.* [72, 109]

Since AlN and GaN are wurtzite crystals with unit cells of only four atoms, their results are expected to resemble experimental studies. On the other hand, $AlGaN$ being an alloy and β-form Ga_2O_3 having 20 atoms and multiple asymmetries in its unit cell; they both represent challenges in theoretical modeling. Following sections will include their results and comparisons.

3.3. $AlGaN$

As it was mentioned before in introduction chapter, $AlGaN$ is an alloy which is frequently produced via introduction of Al atoms to GaN lattice by bringing AlN films in contact with GaN lattice. Therefore, this study also modeled $AlGaN$ as Al atoms residing in GaN lattice as seen in Figure 3.8. This corresponds to a ratio of 3:1 Ga atoms to Al atoms, then the modeled structure is $Al_{0.25}Ga_{0.75}N$. A challenge here is to compare the structure with its counterparts in literature: this exact ratio

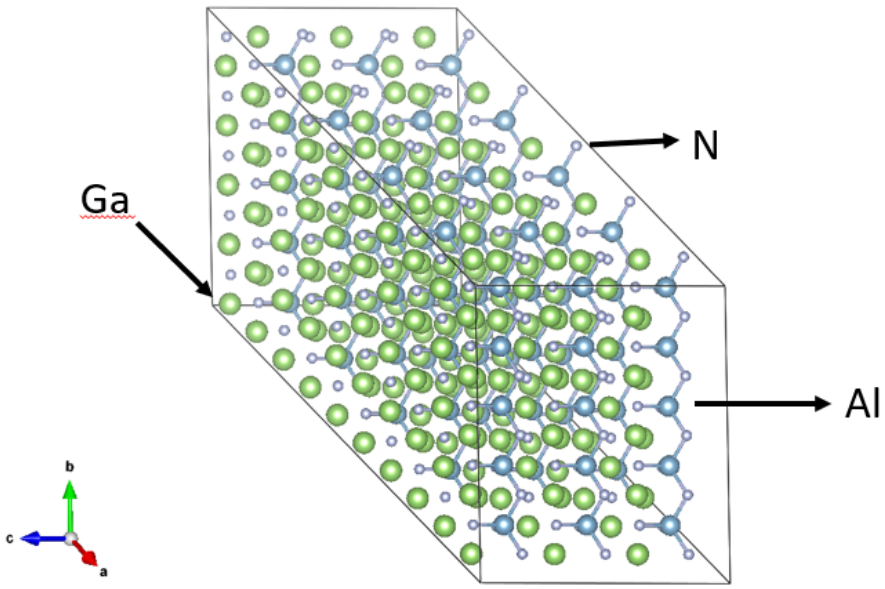

Figure 3.8. Schematic of $Al_{0.25}Ga_{0.75}N$ structure where Al atoms are uniformly distributed in supercell.

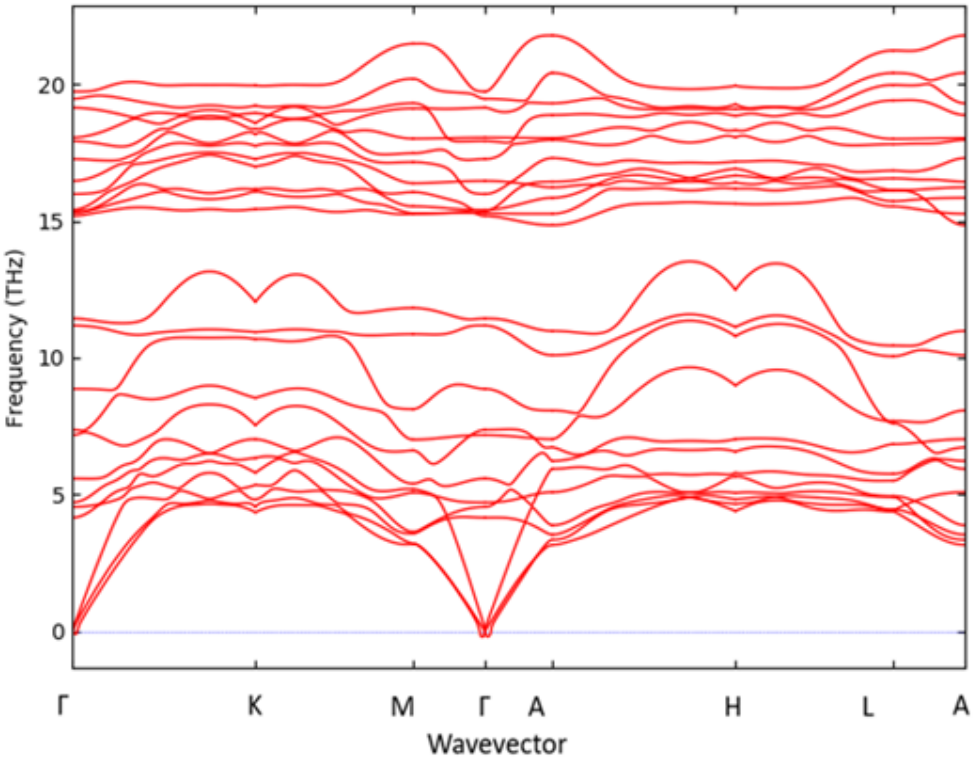

Figure 3.9. Phonon dispersion of $Al_{0.25}Ga_{0.75}N$.

is rarely found; thus, samples with close proportions are chosen in order to have a better comparison. Moreover, since this work replicates the predetermined unit cell, distribution of AlN atoms is considered as homogenous. This may not be the case in experimental set ups since preparing uniform $AlGaN$ alloys is a challenging process. The difference in uniformity is expected to create deviations between experimental and theoretical results.

$AlGaN$ unit cell was transformed into a $2 \times 2 \times 1$ supercell for both third and second order force constants calculations. Since the structure was more complex than the previous ones, a larger cut off of 3.2 $\mathring{A}$ was chosen. Thus, more interactions were considered. Finally, thermal calculations were performed via $20 \times 20 \times 18$ mesh. Phonon dispersion relation of $AlGaN$ was also plotted as seen in Figure 3.9.

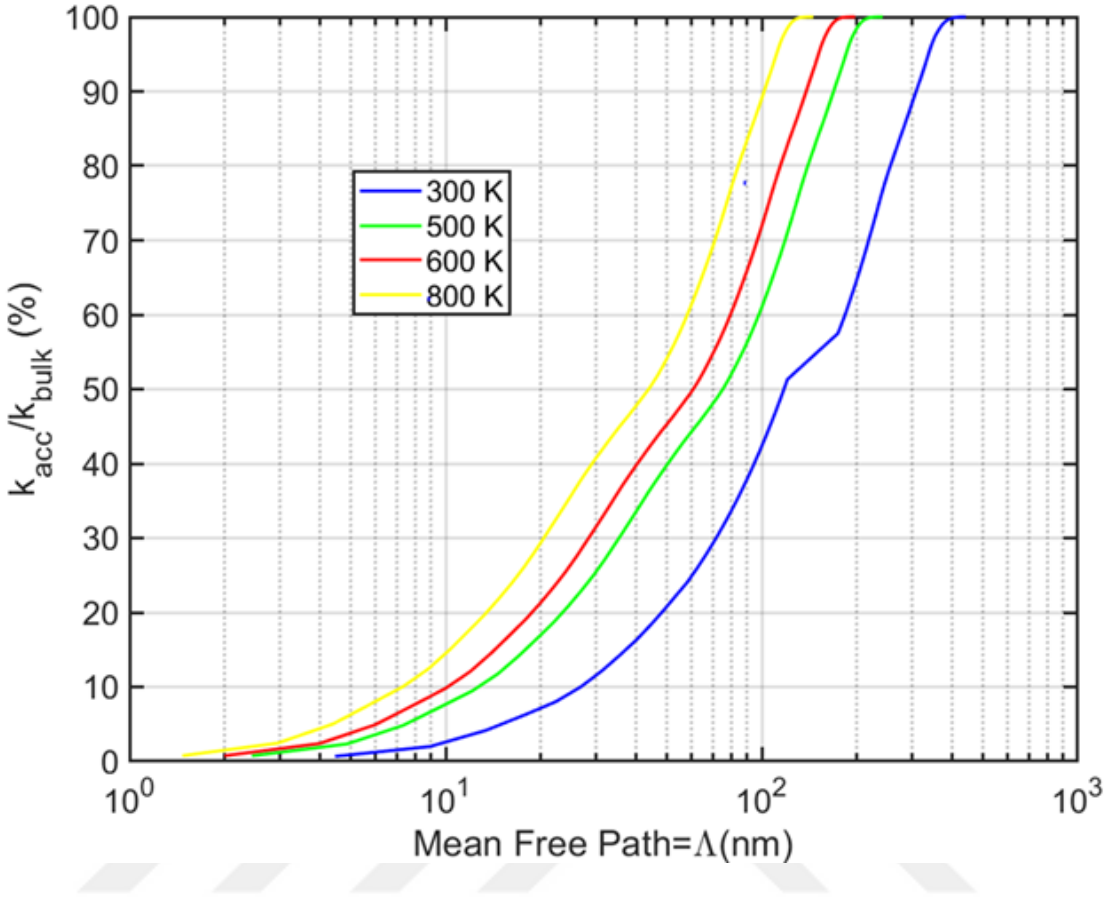

Figure 3.10. Accumulation spectra vs MFP results of $AlGaN$ at 300 K, 500 K, 600 K and 800 K.

As seen in Figure 3.10, $Al_{0.25}Ga_{0.75}N$ is modeled at 300 K, 500 K, 600 K and 800 K. Bulk thermal conductivities are reached as 214.6 W/m-K, 125.3 W/m-K,104.0 W/m-K and finally, 77.8 W/m-K, respectively. Liu & Balandin report 60 W/m-K at 300 K for $Al_{0.23}Ga_{0.77}N$ in cross sectional direction [97]. At 300 K, this study reaches 80.34 W/m-K, 97.6 W/m-K in and 36.7 W/m-K at three crystallographic directions which corresponds to 33%, 62% and 38% deviation from Balandin's data. Critical MFP values are noted in Table 3.3. MFP spectra of $AlGaN$ is significantly shorter than both AlN and GaN, implying that size effects are visible at lower scales.

To compare the accumulation findings, Mitterhuber *et al.*'s work was employed [69]. This work includes accumulation plots and TDTR findings as it can be observed in Figure 3.11. To compare accumulation, Mitterhuber *et al.*'s Holland approach was

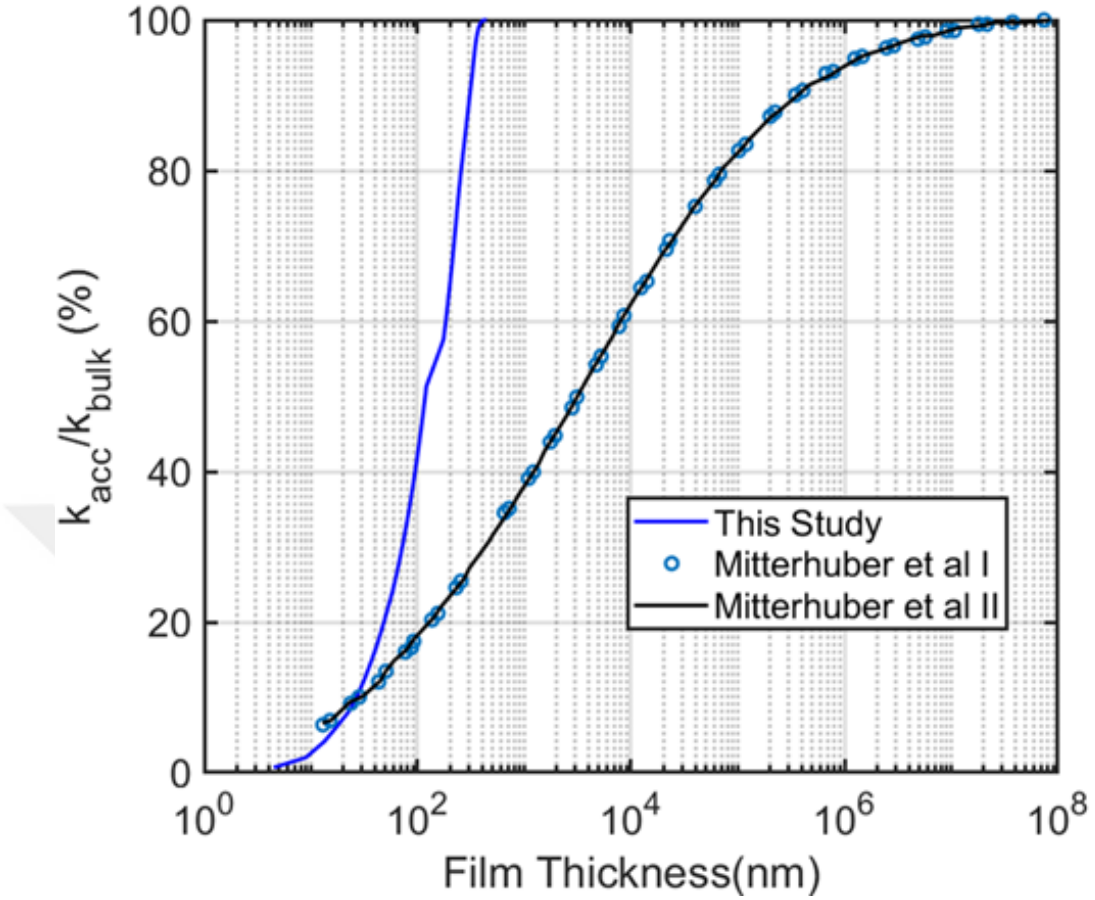

Figure 3.11. Accumulation spectra of $AlGaN$ at 300 K, comparison with Mitterhuber *et al.*'s work [69].

Table 3.3. MFP of phonons contributing to 30%, 50%, and 90% of bulk wurtzite $Al_{0.25}Ga_{0.75}N$ thermal conductivity (k) at various temperatures.

Temperature (Kelvin)	**30% of k**	**50% of k**	**90% of k**	**Total (100%) of k**
300	>72 nm	>117.5 nm	>308 nm	<442.3 nm
500	>36 nm	>75.5 nm	>169 nm	<241.4 nm
600	>28.5 nm	>60.6 nm	>138 nm	<197.6 nm
800	>20.5 nm	>44 nm	>102 nm	<145.5 nm

chosen for two samples: $Al_{0.32}Ga_{0.68}N$ and $Al_{0.17}Ga_{0.83}N$. Though these structures differ in terms of Al concentration, their MFP (also noted as film thickness) spectra are similar. Results of this work reports shorter MFP values than this reference: while theoretical approach of Mitterhuber *et al.* assume that phonons will continue to contribute to thermal conductivity after 0.074 m, this study concludes that total MFP spectrum is only 442.3 nm at 300 K as it is described in Table 3.3. However, this theoretical approach has the risk of oversimplifying phonon interactions.

3.4. β-form Ga_2O_3

Beta Form Gallium Oxide is the fourth and last material of this work and is examined in its closed pack form. Five forms of it can be found: α (rhombohedral), β (monoclinic), γ (cubic), δ (body-centered cubic), and ϵ (orthorhombic). Occasionally, transitionary $\kappa - Ga_2O_3$ is added to this polymorph list [50]. Amongst this polymorph family, the second form which is a member of C2/m space group and is called $\beta - Ga_2O_3$ is our focus as it is reported as the most stable form [50]. β-form Ga_2O_3 has 20 atoms in its unit cell. Despite being the most stable form of Ga_2O_3 family, its unit cell is home to multiple complexities: oxide ions are positioned in an almost cubic arrangement while Ga ions are in octagonal and tetrahedral arrangements. Existence of such disorders and asymmetries results in high anisotropy and certain challenges in both ab-initio and thermal calculations. Calculation processes of β-form Ga_2O_3 is very time consuming, hence coarser calculation steps are taken.

Lattice constants of β-form Ga_2O_3 are defined as $a = 6.414$ $\mathring{A}$ and $c = 5.876$ $\mathring{A}$. Unit cell is not changed to supercell since it is a fairly large unit cell (i.e. $1 \times 1 \times 1$ supercell is constructed). However, even though the unit cell was not completely replicated, a structure of 50 atoms was constructed to ensure periodicity. Thermal calculations are realized via $12 \times 12 \times 12$ mesh. Since unit cell was not replicated in order to avoid excessive computational time, cut-off distance was not introduced to the structure: Every interaction is considered.

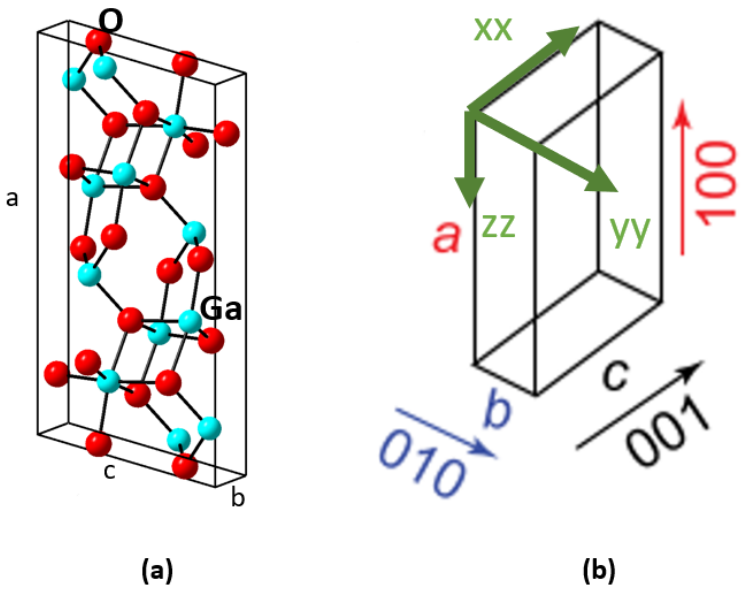

Figure 3.12. Crystallographic directions of β-form Ga_2O_3 unit cell with (a)atoms shown (b)cell is shown [70].

High anisotropy of β-form Ga_2O_3 is frequently reported in literature. While growing crystals and thin films, the growing direction is of crucial importance. Since $\beta-Ga_2O_3$ is highly anisotropic, growth direction immensely affects the properties of final product [3,70]. Directions used in this study and in literature are shown in Figure 3.12. When a work has different notation of directions, corresponding direction is considered for comparison. It can also be observed in Figure 3.13 that accumulation spectra of β-form Ga_2O_3 is highly dependent on directions. Results in Figure 3.13 are calculated at 300 K. It is visible that yy ([010]) direction is the dominant direction in terms of both accumulation behavior and bulk conductivity. Since this direction outweighs other directions in thermal conductivity and is also the frequent thin film growth direction, it is accepted as the reference direction for this material. Accumulation spectra and conductivity calculations are evaluated using this direction.

Bulk conductivity of β-form Ga_2O_3 is found as 29 W/m-K at 300 K, 22.4 W/m-K at 500 K and 15.6 W/m-K at 800 K, respectively. At this study and in the literature, conductivity is dominated by [010], i.e. yy direction as seen in Figure 3.12. This study

Table 3.4. MFP of phonons contributing to 30%, 50%, and 90% of β-form Ga_2O_3 (in dominant yy direction) thermal conductivity (k) at various temperatures.

Temperature (Kelvin)	**30% of k**	**50% of k**	**90% of k**	**Total (100%) of k**
300	>7.3 nm	>25.5 nm	>316.5 nm	<467.9 nm
500	>6.6 nm	>27.5 nm	>216 nm	<305.2 nm
800	>4.9 nm	>30 nm	>140 nm	<197 nm

found the bulk conductivity in this direction to be 22.25 W/m-K. This differs very slightly from Guo *et al.*'s work who report it as 22 W/m-K [70]. This result is also in accordance with Santia *et al.*'s theoretical work, as they report conductivity in this direction as 21.54 W/m-K [87]. Accumulation spectra of β-form Ga_2O_3 are visible in Figure 3.14. MFP of thermally conductive phonons at different ratios are described in Table 3.4.

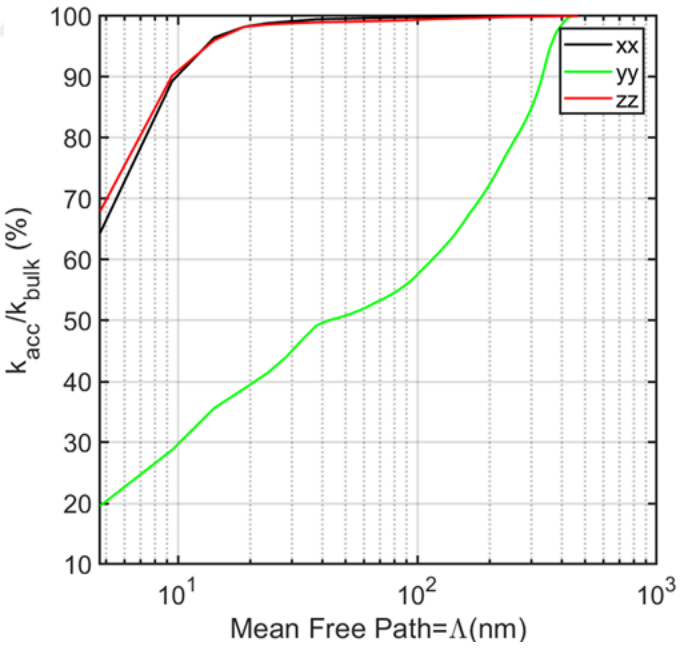

Figure 3.13. Accumulation spectra vs MFP results of three cartesian directions of β-form Ga_2O_3 at 300 K.

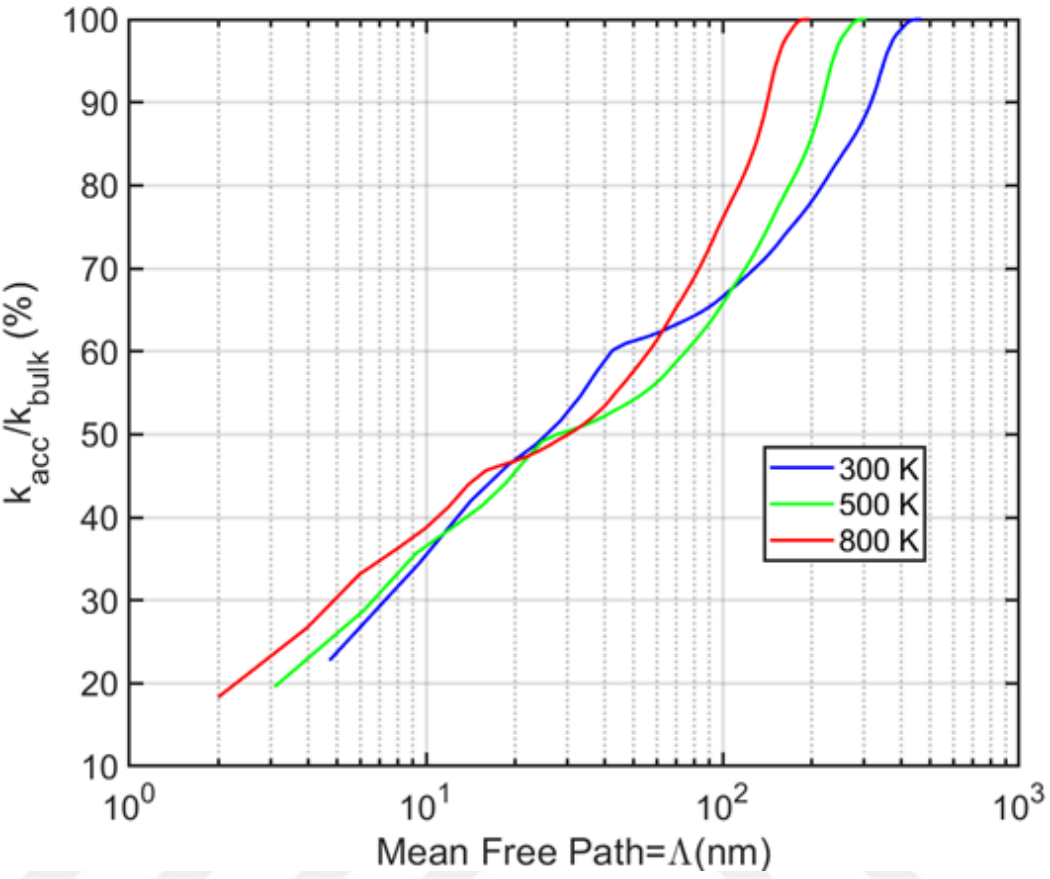

Figure 3.14. Accumulation spectra of β-form Ga_2O_3 in yy ([010]) direction at 300 K, 500 K and 800 K.

β-form Ga_2O_3 is found to have a short spectrum in contrast to AlN and GaN. This stems from not only material properties, but also from asymmetries in crystal. Since GaN and AlN are simpler and ordered structures, an obstruction of phonons in the lattice is unlikely.

When β-form Ga_2O_3 is added, accumulation spectra of all four materials are as seen in Figure 3.15. As expected, AlN and GaN have the longest MFP spectrum. These materials are expected to experience size effects at larger scales. Main cause of this is the ordered and symmetrical structure of their lattice: harmonic behavior is easily observed in these materials. Since phonons can travel longer distances, their MFP is expected to increase. As impurities (such as Al atom in GaN structure) are

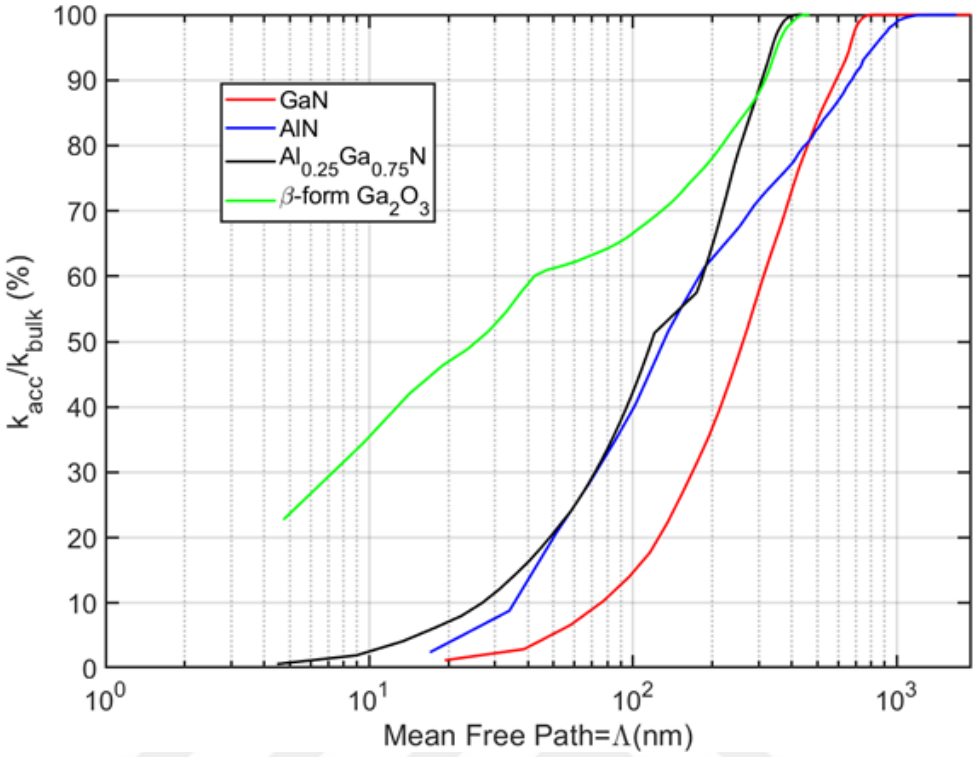

Figure 3.15. Accumulation spectra of GaN, AlN, $Al_{0.25}Ga_{0.75}N$ and β-form Ga_2O_3 (yy direction) at 300 K.

introduced, MFP spectrum shortens due to increased obstacles in lattice. Same interpretation is also applicable to β-form Ga_2O_3, which, yields quite short accumulation spectra due to its complex lattice.

4. THIN FILM APPLICATIONS

This section aims to assess the findings of this work in the light of thin film studies. Previous section has provided normalized accumulation spectra of four materials. This section presents thin film conductivity examples from literature and compares them with accumulation spectra deductions of this study. To obtain thin film reduction ratio, one can simply follow guidelines in accumulation spectra. For instance, *AlN* spectra can be read as seen in Figure 4.1: a guideline of 50% shows which MFP length covers half of the thermal conductivity contribution. Using these data, following deduction can be made: If an *AlN* device layer with a thickness of 77 nm is used at 400 K, half of the bulk conductivity will be lost. If thermal conductivity is not normalized, comparison can directly be performed in terms of conductivity (W/m-K) instead of percentage.

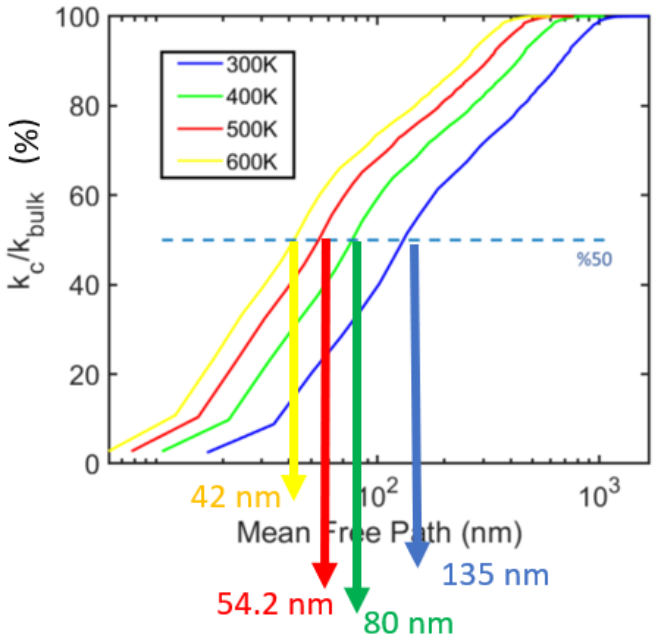

Figure 4.1. *AlN* accumulation spectra showing MFP values contributing to half of the conductivity.

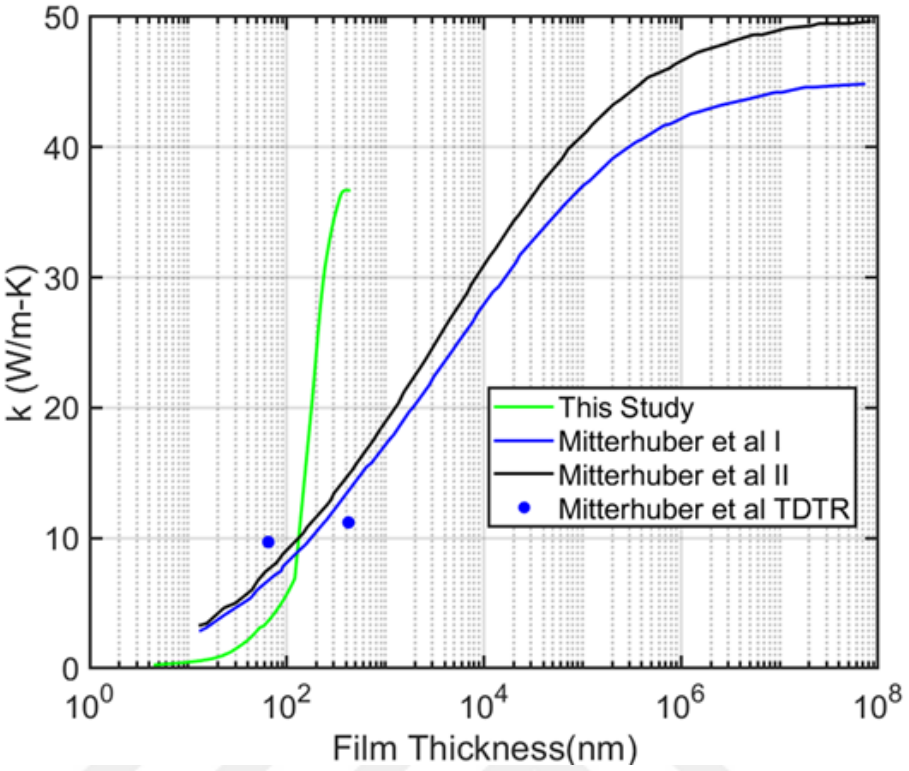

Figure 4.2. Thermal conductivity(non-normalized) vs film thickness results of *AlGaN* at 300 K, comparison with Mitterhuber *et al.*'s work [69].

When it comes to comparison with the literature, thin film thermal conductivity reduction in *AlN* case is already visible in Figure 3.7. Park and Kim's experimental work on thin films yield 50% reduction of *AlN* bulk conductivity. They measured thermal conductivity via xenon flash instrument [109]. However, while this study reports 50% thermal conductivity reduction at 135 nm, Park and Kim predicts it to happen at 200 nm.

A further comparison in terms of thin film thermal conductivity can be observed in Figure 4.2. Here, *AlGaN* conductivity is not normalized in order to compare cross sectional bulk conductivity with Mitterhuber *et al.*'s work. Moreover, their TDTR findings are also added. TDTR findings are in better agreement with this work than Holland approach, as seen in Figure 4.2. However,as it was previously discussed, TDTR experiments entail multiple uncertainties. Finally, it can be deduced that at short

MFP range, phonon entrapment results in increased anharmonicity since more phonons collide. Thus, covering further steps of ground energy is expected to explain thermal accumulation behavior more accurately.

As for GaN , experimental work of Cho *et al.* (2012) report 63% reduction in thermal conductivity at 150 nm and a range of 18-35% reduction at 800 nm [110]. Referring to GaN accumulation spectrum of this study, conductivity loss is 74% and 0.1% at these scales. Moreover, Koh *et al.* determined the conductivity loss to be 50% at 690 nm and 20% at 3600 nm [111]. This study finds that at 690 nm, only 4% of conductivity is compromised and at 3600 nm, conductivity loss does not occur. On the other hand, harmonic approximation shown in Chapter 3 reports 83% at 150 nm, 15% reduction at 690 nm ,12% reduction at 800 nm and 1% reduction at 3600 nm.

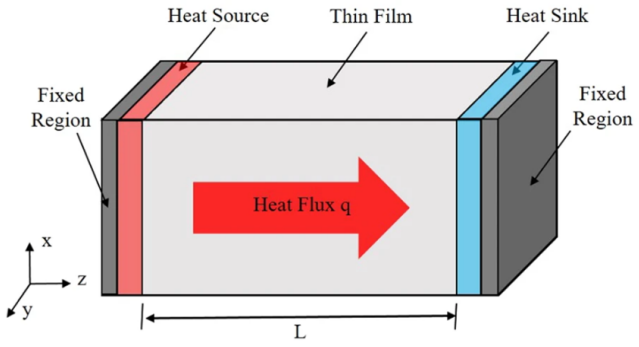

Figure 4.3. Thin film model of NEMD method. [112]

Since multiple discrepancies and unknown parameters are involved in experimental processes such as fitting parameters and sample properties,a healthy comparison is difficult. Comparison with theoretical models should also be involved. A robust method of modeling thin film conductivity is NEMD (non-equilibrium molecular dynamics) method. This study is compared to a GaN NEMD work in an attempt to evaluate thin film conductivity findings. Briefly, NEMD method makes use of Fourier equation (described in Equation 2.10) to model temperature difference and thermal conductivity k. As seen in Figure 4.3, NEMD models an infinite thin film, hence operates on 2D. In this study, heat is assumed to flow through the length L of thin film. To obtain behavior at 300 K, 500 K and 800 K, heat source and heat sink pairs are de-

termined as 310 K-290 K, 515 K-500 K, and 820 K-800 K . Stillinger-Weber potentials are employed with Bere and Serra's parameters [113–115] .

As seen in Figure 4.4, both methods yield similar results for GaN. Moreover, conductivities at different temperatures are found to be quite similar to this work: NEMD reports 226.95 W/m-K, 138.59 W/m-K and 88.35 W/m-K at 300 K, 500 K, and 800 K, respectively. However, NEMD method resides on building thin film samples of a predetermined size. Thus, continuous accumulation results cannot be obtained via NEMD as observed in Figure 4.4. NEMD data here are represented in points. NEMD results also predict longer MFP spectra, since it heavily depends on used potentials and imposed boundary conditions. Therefore, rather than considering phonon interactions at that scale, NEMD resides on electronic potentials and falls short in considering

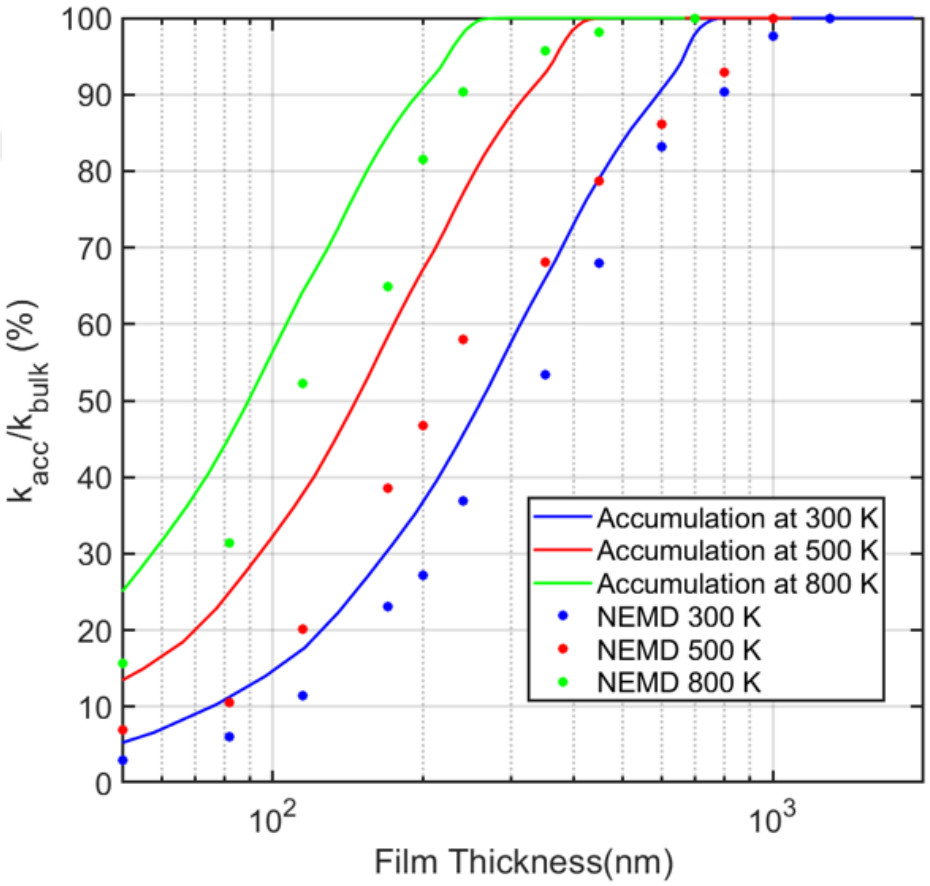

Figure 4.4. Comparison of NEMD work with ab-initio results of this study.

phonon interactions. Finally, another reason behind MFP discrepancy between NEMD and ab-initio results of this work is that NEMD overlooks third dimension as seen in Figure 4.3. Since NEMD method performs its calculations via installment of thermostats on a modeled, infinite 2D film, out of plane phonon interactions are likely to be neglected.

5. CONCLUSIONS & IMPLICATIONS FOR FUTURE RESEARCH

Accumulation spectra of wide and ultra-wide bandgap materials GaN, AlN, $Al_{0.25}Ga_{0.75}N$ and β-form Ga_2O_3 are calculated. Results at different temperatures are provided. Bulk thermal conductivities and accumulation spectra are compared to examples in literature. Results are analyzed and discrepancies with literature were discussed. A method was devised in order to interpret accumulation spectrum in the aspect of thermal conductivity reduction. Thermal conductivity values of confined structures were inferred from accumulation spectra and were compared with the instances in literature.

The main objective of obtaining accumulated thermal conductivity-MFP relation is to predict thermal behavior of materials at small scales such as thin films and localized hotspots. These data were provided in terms of critical MFP-thermal conductivity contribution tables. It was found that materials with simple structures have longer MFP spectra than materials with asymmetric crystallographic properties. It was also found that existence of impurities shortens the MFP spectrum as it is the case for $AlGaN$.

It was concluded that as anharmonicity increases, usage of third order force constants becomes crucial. Third order force constants help cover a larger part of crystal energy approximation function; therefore, it offers a further description of crystal's state. This renders their employment beneficial in terms of covering more than solely harmonic situations. In the existence of impurities, dislocations, stresses and increased temperature, lattice becomes disordered. Phonon interaction increases, hence anharmonic behavior occurs. Therefore, in these situations, it is logical to adopt third order force constants in order to predict thermal behavior.

As anharmonicity and disorder increases, it was seen that MFP accumulation function becomes steeper. This results in sudden changes in thermal conductivity at small scales. One entailment of this is that one can expect sudden decrease in thermal conductivity when working with a material of short MFP spectrum. This problem aggravates in high temperature conditions since MFP spectrum shortens as temperature rises. Hence, when using a material with short MFP spectrum in a nano or micro scale structure, one should design more carefully.

Differences between experimental works and theoretical methods are estimated to have their roots in modeled samples as well as experimental hardships: while an experimental sample has cracks, dislocations, and unintended dopants; theoretical models frequently assume a perfect crystal. Moreover, experimental uncertainties also play a role. Experimental works are not independent from approximations and they also suffer from uncertainties entailed by fitting. It was also seen that, as it is the case in β-form Ga_2O_3 , certain materials present challenges in thin film production and measurements; then fluctuation occurs in experimental results. However, using third order force constants underestimate MFP spectrum even in comparison to other theoretical approaches. This may stem from overestimation of phonon interactions. Therefore, the best use of employing this method is to model situations where phonon interaction ratio is high. Instances of these cases are increased temperature, existence of impurities and dislocations as well as structures where phonons are trapped, i.e. localized hotspots and thin films.

Even though this work yields a continuous spectrum and does not necessitate repeated calculations, future aspects of this research still needs reduction of calculation time. Then, cut-off distance might be eliminated, and larger supercells can be modeled. With more computational power, modeling of structures other than perfect crystals will become easier. It will be possible to model dislocations, impurities and materials with even larger unit cells. To fasten the ab-initio calculations, technologies such as machine learning and deep learning might be adopted since these technologies allow us to process more data in shorter time intervals and to obtain accurate results from fewer data points. Advances in hardware technology is also expected to accelerate

calculations in both ab-initio and thermal field. Moreover, experimental methods such as TDTR and 3ω are also expected to enhance in near future: this will yield healthier comparisons.

The approach of this study is expected to enhance theoretical models in future via helping the detection of size effects. Macro scale finite element analyses cannot function in the presence of size effects due to unknown conductivity. Thermal conductivity output of accumulation spectrum at chosen length scale may be incorporated in these studies: hence, a thorough analysis of complex devices can be achieved. Better device designs and enhanced thermal duration can be realized.

Finally, accumulation spectra are provided for four WBG and UWBG materials AlN, GaN, $AlGaN$ and β-form Ga_2O_3. Accumulation spectra are expected to provide beforehand idea of materials' thermal behavior at small scales. Using these spectra, it is possible to predict at which length scale size effects will dominate and how much of the thermal conductivity will be compromised. Then accumulation spectra free size effect detection from the cost and effort of experimental studies. The method of this study is also a good option when compared to other theoretical approaches which fail to capture thermal conductivity reduction according to length scale thoroughly. Thus, it is expected that this method will help to enhance thermal conductivity analysis in multiple fields.

REFERENCES

1. Tsao, J. Y. and C. *et al.*, "Ultrawide-Bandgap Semiconductors: Research Opportunities and Challenges", *Advanced Electronic Materials*, Vol. 4, No. 1, pp. 1–49, 2018.

2. Scott, M. J., L. Fu, X. Zhang, J. Li, C. Yao, M. Sievers and J. Wang, "Merits of gallium nitride based power conversion", *Semiconductor Science and Technology*, Vol. 28, No. 7, 2013.

3. Baldini, M., Z. Galazka and G. Wagner, "Recent progress in the growth of β-Ga2O3 for power electronics applications", *Materials Science in Semiconductor Processing*, Vol. 78, pp. 132–146, 2018.

4. Ferhat, M. and A. Zaoui, "Do all III-V compounds have the zinc-blende or wurtzite ground state structure?", *Applied Physics Letters*, Vol. 88, No. 16, pp. 1–3, 2006.

5. Briot, O., J. P. Alexis, S. Sanchez, B. Gil and R. L. Aulombard, "Influence of the V/III molar ratio on the structural and electronic properties of MOVPE grown GaN", *Solid-State Electronics*, Vol. 41, No. 2 SPEC. ISS., pp. 315–317, 1997.

6. Xiao, R. F., X. W. Sun, Z. F. Li, N. Cue, H. S. Kwok, Q. Z. Liu and S. S. Lau, "Growth of gallium nitride thin films by liquid-target pulsed laser deposition", *Journal of Vacuum Science & Technology A: Vacuum, Surfaces, and Films*, Vol. 15, No. 4, pp. 2207–2213, 1997.

7. Razzak, T., H. Xue, Z. Xia, S. Hwang, A. Khan, W. Lu and S. Rajan, "Ultra-wide band gap materials for high frequency applications", *2018 IEEE MTT-S International Microwave Workshop Series on Advanced Materials and Processes for RF and THz Applications, IMWS-AMP*, pp. 1–3, 2018.

8. Wu, Y. F., "Paralleling high-speed GaN power HEMTs for quadrupled power output", *Proceedings of the IEEE Applied Power Electronics Conference and Exposition - APEC*, pp. 211–214, 2013.

9. Tian, J., C. Lai, G. Feng, D. Banerjee, W. Li and N. C. Kar, "Review of recent progresses on gallium nitride transistor in power conversion application", *International Journal of Sustainable Energy*, Vol. 39, No. 1, pp. 88–100, 2020.

10. Ding, X., Y. Zhou and J. Cheng, "A Review of Gallium Nitride Power Device and Its Applications in Motor Drive", *China Electrotechnical Society Transactions on Electrical Machines and Systems*, Vol. 3, No. 1, pp. 54–64, 2019.

11. Wu, Y. F., R. Coffie, N. Fichtenbaum, Y. Dora, C. S. Suh, L. Shen, P. Parikh and U. K. Mishra, "Total GaN solution to electrical power conversion", *Device Research Conference - Conference Digest, DRC*, pp. 217–218, 2011.

12. Liang, Y. C., G. S. Samudra, H. Huang, C. F. Huang and T. F. Chang, "AlGaN/GaN power HEMT devices for future energy conversion applications", *ISNE 2013 - IEEE International Symposium on Next-Generation Electronics 2013*, pp. 7–10, 2013.

13. Donmezer, F. N., *Multiscale electro-thermal modeling of AlGaN/GaN heterostructure field effect transistors*, Ph.D. Thesis, Georgia Institute of Technology, 2013.

14. Cicek, B., N. Sahin and M. Alkan, "Thermal analysis of chip on board packaging of high power led's with heat pipe using Cfd for street lights", *Gazi University Journal of Science*, Vol. 31, No. 4, pp. 1229–1244, 2018.

15. Kara, D., N. Donmezer, T. F. Canan, O. Sen and E. Ozbay, "Effects of field plate on the maximum temperature and temperature distribution for gan HEMT devices", *ASME 2016 Heat Transfer Summer Conference, HT 2016, collocated with the ASME 2016 Fluids Engineering Division Summer Meeting and the ASME 2016 14th International Conference on Nanochannels, Microchannels, and*

Minichannels, Vol. 1, pp. 1–7, American Society of Mechanical Engineers, 2016.

16. Russell, S. A., A. Perez-Tomas, C. F. McConville, C. A. Fisher, D. P. Hamilton, P. A. Mawby and M. R. Jennings, "Heteroepitaxial Beta-Ga2O3 on 4H-SiC for an FET with Reduced Self Heating", *IEEE Journal of the Electron Devices Society*, Vol. 5, No. 4, pp. 256–261, 2017.

17. Acharya, A. R., "Group III – Nitride Semiconductors: Preeminent Materials for Modern Electronic and Optoelectronic Applications", *Himalayan Physics*, Vol. 5, pp. 22–26, 2015.

18. Khan, M. A., J. N. Kuznia, D. T. Olson, J. M. Van Hove, M. Blasingame and L. F. Reitz, "High-responsivity photoconductive ultraviolet sensors based on insulating single-crystal GaN epilayers", *Applied Physics Letters*, Vol. 60, No. 23, pp. 2917–2919, 1992.

19. Dylewicz, R., S. Z. Patela and R. Paszkiewicz, "Applications of GaN-based materials in modern optoelectronics", *Photonics Applications in Astronomy, Communications, Industry, and High-Energy Physics Experiments II*, Vol. 5484, pp. 328 – 335, International Society for Optics and Photonics, SPIE, 2004.

20. Leung, T. T. and C. W. Ong, "Nearly amorphous to epitaxial growth of aluminum nitride films", *Diamond and Related Materials*, Vol. 13, No. 9, pp. 1603–1608, 2004.

21. Alrashdan, M. H., A. A. Hamzah, B. Y. Majlis and M. F. Aziz, "Aluminum nitride thin film deposition using DC sputtering", *IEEE International Conference on Semiconductor Electronics, Proceedings, ICSE*, pp. 72–75, 2014.

22. Iqbal, A. and F. Mohd-Yasin, "Reactive sputtering of aluminum nitride (002) thin films for piezoelectric applications: A review", *Sensors (Switzerland)*, Vol. 18, No. 6, pp. 1–21, 2018.

23. Xu, R. L., M. Munõz Rojo, S. M. Islam, A. Sood, B. Vareskic, A. Katre, N. Mingo, K. E. Goodson, H. G. Xing, D. Jena and E. Pop, "Thermal conductivity of crystalline AlN and the influence of atomic-scale defects", *Journal of Applied Physics*, Vol. 126, No. 18, pp. 1–7, 2019.

24. Zollner, C. J., A. Almogbel, Y. Yao, B. K. Saifaddin, F. Wu, M. Iza, S. P. Denbaars, J. S. Speck and S. Nakamura, "Reduced dislocation density and residual tension in AlN grown on SiC by metalorganic chemical vapor deposition", *Applied Physics Letters*, Vol. 115, No. 16, pp. 1–5, 2019.

25. Foronda, H. M., F. Wu, C. Zollner, M. E. Alif, B. Saifaddin, A. Almogbel, M. Iza, S. Nakamura, S. P. DenBaars and J. S. Speck, "Low threading dislocation density aluminum nitride on silicon carbide through the use of reduced temperature interlayers", *Journal of Crystal Growth*, Vol. 483, pp. 134–139, 2018.

26. Franco Júnior, A. and D. J. Shanafield, "Thermal conductivity of polycrystalline aluminum nitride (AlN) ceramics", *Cerâmica*, Vol. 50, No. 315, pp. 247–253, 2005.

27. Fu, X., "Aluminum Nitride Wide Band-gap Semiconductor and Its Basic Characteristics", *Proceedings of the 6th International Conference on Electronic, Mechanical, Information and Management Society*, pp. 555–558, Atlantis Press, Paris, France, 2016.

28. Chu, B. H., B. S. Kang, S. C. Hung, K. H. Chen, F. Ren, A. Sciullo, B. P. Gila and S. J. Pearton, "Aluminum gallium nitride (GaN)/GaN high electron mobility transistor-based sensors for glucose detection in exhaled breath condensate", *Journal of Diabetes Science and Technology*, Vol. 4, No. 1, pp. 171–179, 2010.

29. Khan, A., K. Balakrishnan and T. Katona, "Ultraviolet light-emitting diodes based on group three nitrides", *Nature Photonics*, Vol. 2, No. 2, pp. 77–84, 2008.

30. Lee, T. H., B. R. Lee, K. R. Son, H. W. Shin and T. G. Kim, "Highly Efficient Deep-UV Light-Emitting Diodes Using AlN-Based Deep-UV-Transparent Glass

Electrodes", *ACS Applied Materials and Interfaces*, Vol. 9, No. 50, pp. 43774–43781, 2017.

31. Dubois, M. A. and P. Muralt, "Properties of aluminum nitride thin films for piezoelectric transducers and microwave filter applications", *Applied Physics Letters*, Vol. 74, No. 20, pp. 3032–3034, 1999.

32. Ren, Z., Q. Sun, S. Y. Kwon, J. Han, K. Davitt, Y. K. Song, A. V. Nurmikko, H. K. Cho, W. Liu, J. A. Smart and L. J. Schowalter, "Heteroepitaxy of AlGaN on bulk AlN substrates for deep ultraviolet light emitting diodes", *Applied Physics Letters*, Vol. 91, No. 5, 2007.

33. Zhang, J., Y. Gao, L. Zhou, Y.-U. Gil and K.-M. Kim, "Transparent deep ultraviolet light-emitting diodes with a p-type AlN ohmic contact layer", *Light-Emitting Devices, Materials, and Applications*, Vol. 10940, pp. 1–8, SPIE, 2019.

34. Taniyasu, Y., M. Kasu and T. Makimoto, "An aluminium nitride light-emitting diode with a wavelength of 210 nanometres", *Nature*, Vol. 441, No. 7091, pp. 325–328, 2006.

35. Li, Y., M. Dvořák, P. N. Nesterenko, N. Nuchtavorn and M. Macka, "High power deep UV-LEDs for analytical optical instrumentation", *Sensors and Actuators, B: Chemical*, Vol. 255, pp. 1238–1243, 2018.

36. Shatalov, M., A. Lunev, X. Hu, O. Bilenko, I. Gaska, W. Sun, J. Yang, A. Dobrinsky, Y. Bilenko, R. Gaska and M. Shur, "Performance and applications of deep UV LED", Vol. 21, No. 1, pp. 1–6, 2012.

37. Muramoto, Y., M. Kimura and S. Nouda, "Development and future of ultraviolet light-emitting diodes: UV-LED will replace the UV lamp", *Semiconductor Science and Technology*, Vol. 29, No. 8, pp. 1–8, 2014.

38. Rodak, L. E. and D. Korakakis, "Aluminum gallium nitride alloys grown via

metalorganic vapor-phase epitaxy using a digital growth technique", *Journal of Electronic Materials*, Vol. 40, No. 4, pp. 388–393, 2011.

39. Stutzmann, M., O. Ambacher, H. Angerer, C. Nebel and E. Rohrer, "Electrical and structural properties of AlGaN: A comparison with CVD diamond", *Diamond and Related Materials*, Vol. 7, No. 2-5, pp. 123–128, 1998.

40. Xin Jing, H., C. A. Che Abdullah, M. Z. Mohd Yusoff, A. Mahyuddin and Z. Hassan, "Structural and optical properties of AlN/GaN and AlN/AlGaN/GaN thin films on silicon substrate prepared by plasma assisted molecular beam epitaxy (MBE)", *Results in Physics*, Vol. 12, pp. 1177–1181, 2019.

41. Saxler, A., W. C. Mitchel, P. Kung and M. Razeghi, "Aluminum gallium nitride short-period superlattices doped with magnesium", *Applied Physics Letters*, Vol. 74, No. 14, pp. 2023–2025, 1999.

42. Xiaobin, L., L. Yuanjie, Y. Weihua, L. Xin, D. Shaobo and F. Zhihong, *Designing AlGaN/GaN HEMTs for W-Band*, 2014, `https://www.mwrf.com/technologies/semiconductors/article/21845779`, Last accessed on 2020-07-05.

43. Mishra, U. K., P. Parikh and Y. F. Wu, "AlGaN/GaN HEMTs - An overview of device operation and applications", *Proceedings of the IEEE*, Vol. 90, No. 6, pp. 1022–1031, 2002.

44. Venkatachalam, A., W. T. James and S. Graham, "Electro-thermo-mechanical modeling of GaN-based HFETs and MOSHFETs", *Semiconductor Science and Technology*, Vol. 26, No. 8, pp. 85027–85033, 2011.

45. Das, S., A. K. Panda and G. N. Dash, "Characterization of electrical properties of AlGaN/GaN interface using coupled Schrödinger and Poisson equation", *Journal of Semiconductors*, Vol. 33, No. 11, pp. 62–70, 2012.

46. Krishna, A., A. Raj, N. Hatui, O. Koksaldi, R. Jang, S. Keller and U. K. Mishra, "AlGaN/GaN Superlattice-Based p-Type Field-Effect Transistor with Tetramethylammonium Hydroxide Treatment", *Physica Status Solidi (A) Applications and Materials Science*, Vol. 217, No. 7, pp. 1–8, 2020.

47. Syaranamual, G. J., W. A. Sasangka, R. I. Made, S. Arulkumaran, G. I. Ng, S. C. Foo, C. L. Gan and C. V. Thompson, "Role of two-dimensional electron gas (2DEG) in AlGaN/GaN high electron mobility transistor (HEMT) ON-state degradation", *Microelectronics Reliability*, Vol. 64, pp. 589–593, 2016.

48. Shatalov, M., W. Sun, R. Jain, A. Lunev, X. Hu, A. Dobrinsky, Y. Bilenko, J. Yang, G. A. Garrett, L. E. Rodak, M. Wraback, M. Shur and R. Gaska, "High power AlGaN ultraviolet light emitters", *Semiconductor Science and Technology*, Vol. 29, No. 8, pp. 8–13, 2014.

49. Tran, B. T. and H. Hirayama, "Growth and Fabrication of High External Quantum Efficiency AlGaN-Based Deep Ultraviolet Light-Emitting Diode Grown on Pattern Si Substrate", *Scientific Reports*, Vol. 7, No. 1, pp. 1–6, 2017.

50. Romanov, A. E., S. I. Stepanov, V. I. Nikolaev and V. E. Bougrov, "Gallium Oxide: Properties and Applica 4 98 a Review", *Reviews on Advanced Materials Science*, Vol. 44, pp. 63–86, 2016.

51. Marie, P., X. Portier and J. Cardin, "Growth and characterization of gallium oxide thin films by radiofrequency magnetron sputtering", *Physica Status Solidi (A) Applications and Materials Science*, Vol. 205, pp. 1943–1946, 2008.

52. Pearton, S. J., J. Yang, P. H. Cary, F. Ren, J. Kim, M. J. Tadjer and M. A. Mastro, "A review of Ga2O3 materials, processing, and devices", *Applied Physics Reviews*, Vol. 5, No. 1, pp. 1–51, 2018.

53. Kim, J., S. Oh, J. Kim, F. Ren and S. J. Pearton, "Quasi-two-dimensional β-gallium oxide solar-blind photodetectors with ultrahigh responsivity", *Journal of*

Materials Chemistry C, Vol. 4, No. 39, pp. 9245–9250, 2016.

54. Pratiyush, A. S., S. Krishnamoorthy, R. Muralidharan, S. Rajan and D. N. Nath, *Gallium Oxide: Technology, Devices and Applications*, Elsevier, 2018.

55. Winter, R., *Dispersion relations :Condensed Matter Physics*, 2011, `https://users.aber.ac.uk/ruw/teach/334/disprel.php`, Last accessed on 2020-07-12.

56. Lindsay, L., D. A. Broido and T. L. Reinecke, "Thermal Conductivity and Large Isotope Effect in GaN from First Principles", *Physical Review Letters*, Vol. 109, No. 9, pp. 1–4, 2012.

57. Shukla, G., *Impossibility of the Simple Cubic Metal in Nature*, 2018, `researchgate.net/publication/324113293`, Last accessed on 2020-07-10.

58. Szwejkowski, C. J., N. C. Creange, K. Sun, A. Giri, B. F. Donovan, C. Constantin and P. E. Hopkins, "Size effects in the thermal conductivity of gallium oxide (β-Ga2O3) films grown via open-atmosphere annealing of gallium nitride", *Journal of Applied Physics*, Vol. 117, No. 8, pp. 1–9, 2015.

59. Beechem, T. E., A. E. McDonald, E. J. Fuller, A. A. Talin, C. M. Rost, J.-P. P. Maria, J. T. Gaskins, P. E. Hopkins and A. A. Allerman, "Size dictated thermal conductivity of GaN", *Journal of Applied Physics*, Vol. 120, No. 9, pp. 1–5, 2016.

60. Hu, Y., L. Zeng, A. J. Minnich, M. S. Dresselhaus and G. Chen, "Spectral mapping of thermal conductivity through nanoscale ballistic transport", *Nature Nanotechnology*, Vol. 10, No. 8, pp. 701–706, 2015.

61. Killat, N., J. W. Pomeroy, J. L. Jimenez and M. Kuball, "Thermal properties of AlGaN/GaN high electron mobility transistors on 4H and 6H SiC substrates", *Physica Status Solidi (A) Applications and Materials Science*, Vol. 211, No. 12, pp. 2844–2847, 2014.

62. Jiang, P., X. Qian and R. Yang, "Tutorial: Time-domain thermoreflectance (TDTR) for thermal property characterization of bulk and thin film materials", *Journal of Applied Physics*, Vol. 124, No. 16, pp. 1–30, 2018.

63. Cahill, D. G. and R. O. Pohl, "Thermal conductivity of amorphous solids above the plateau", *Physical Review B*, Vol. 35, No. 8, pp. 4067–4073, 1987.

64. Cahill, D. G., "Thermal conductivity measurement from 30 to 750 K: The 3ω method", *Review of Scientific Instruments*, Vol. 61, No. 2, pp. 802–808, 1990.

65. Hodges, C., J. Anaya Calvo, S. Stoffels, D. Marcon and M. Kuball, "AlGaN/GaN field effect transistors for power electronics - Effect of finite GaN layer thickness on thermal characteristics", *Applied Physics Letters*, Vol. 103, No. 20, pp. 1–4, 2013.

66. Killat, N., M. Montes, J. W. Pomeroy, T. Paskova, K. R. Evans, J. Leach, X. Li, U. Ozgur, H. Morkoc, K. D. Chabak, A. Crespo, J. K. Gillespie, R. Fitch, M. Kossler, D. E. Walker, M. Trejo, G. D. Via, J. D. Blevins and M. Kuball, "Thermal Properties of AlGaN/GaN HFETs on Bulk GaN Substrates", *IEEE Electron Device Letters*, Vol. 33, No. 3, pp. 366–368, 2012.

67. Sarua, A., J. Hangfeng, M. Kuball, M. J. Uren, T. Martin, K. P. Hilton and R. S. Balmer, "Integrated micro-Raman/infrared thermography probe for monitoring of self-heating in AlGaN/GaN transistor structures", *IEEE Transactions on Electron Devices*, Vol. 53, No. 10, pp. 2438–2447, 2006.

68. Kuball, M., S. Rajasingam, A. Sarua, M. J. Uren, T. Martin, B. T. Hughes, K. P. Hilton and R. S. Balmer, "Measurement of temperature distribution in multifinger AlGaN/GaN heterostructure field-effect transistors using micro-Raman spectroscopy", *Applied Physics Letters*, Vol. 82, No. 1, pp. 124–126, 2003.

69. Mitterhuber, L., R. Hammer, T. Dengg and J. Spitaler, "Thermal Characterization and Modelling of AlGaN-GaN Multilayer Structures for HEMT Applica-

tions", *Energies*, Vol. 13, No. 9, pp. 1–17, 2020.

70. Guo, Z., A. Verma, X. Wu, F. Sun, A. Hickman, T. Masui, A. Kuramata, M. Higashiwaki, D. Jena and T. Luo, "Anisotropic thermal conductivity in single crystal β-gallium oxide", *Applied Physics Letters*, Vol. 106, No. 11, pp. 1–5, 2015.

71. Tran, D. Q., N. Blumenschein, A. Mock, P. Sukkaew, H. Zhang, J. F. Muth, T. Paskova, P. P. Paskov and V. Darakchieva, "Thermal conductivity of ultrawide bandgap thin layers – High Al-content AlGaN and β-Ga2O3", *Physica B: Condensed Matter*, Vol. 579, pp. 1–6, 2020.

72. Freedman, J. P., J. H. Leach, E. A. Preble, Z. Sitar, R. F. Davis and J. A. Malen, "Universal phonon mean free path spectra in crystalline semiconductors at high temperature", *Scientific reports*, Vol. 3, pp. 1–6, 2013.

73. Mion, C., J. F. Muth, E. A. Preble and D. Hanser, "Accurate dependence of gallium nitride thermal conductivity on dislocation density", *Applied Physics Letters*, Vol. 89, No. 9, pp. 1–3, 2006.

74. Avcu, M., R. Sommet, J. P. Teyssier, G. Callet, A. El-Rafei and R. Quéré, "Measurement of thermal impedance of GaN HEMTs using 3ω method", *Electronics Letters*, Vol. 48, No. 12, pp. 708–710, 2012.

75. Bogner, M., A. Hofer, G. Benstetter, H. Gruber and R. Y. Fu, "Differential 3ω method for measuring thermal conductivity of AIN and Si3N4 thin films", *Thin Solid Films*, Vol. 591, pp. 267–270, 2015.

76. Ramu, A. T. and J. E. Bowers, "A compact heat transfer model based on an enhanced Fourier law for analysis of frequency-domain thermoreflectance experiments", *Applied Physics Letters*, Vol. 106, No. 26, pp. 1–4, 2015.

77. Kaiser, J., T. Feng, J. Maassen, X. Wang, X. Ruan and M. Lundstrom, "Thermal transport at the nanoscale: A Fourier's law vs. phonon Boltzmann equation

study", *Journal of Applied Physics*, Vol. 121, No. 4, pp. 1–20, 2017.

78. Miyazaki, K., T. Arashi, H. Tsukamoto, D. Song and G. Chen, "Heat conduction in micro-structured materials", *Thermomechanical Phenomena in Electronic Systems -Proceedings of the Intersociety Conference*, Vol. 2, No. 2, pp. 617–621, 2004.

79. McGaughey, A. J., A. Jain, H. Y. Kim and B. Fu, "Phonon properties and thermal conductivity from first principles, lattice dynamics, and the Boltzmann transport equation", *Journal of Applied Physics*, Vol. 125, No. 1, pp. 1–19, 2019.

80. Gorczyca, I., T. Suski, N. E. Christensen and A. Svane, "Theoretical study of nitride short period superlattices", *Journal of Physics Condensed Matter*, Vol. 30, No. 6, pp. 2–29, 2018.

81. Lindsay, L., D. A. Broido and T. L. Reinecke, "Ab initio thermal transport in compound semiconductors", *Physical Review B - Condensed Matter and Materials Physics*, Vol. 87, No. 16, pp. 1–60, 2013.

82. Jiang, Y., S. Cai, Y. Tao, Z. Wei, K. Bi and Y. Chen, "Phonon transport properties of bulk and monolayer GaN from first-principles calculations", *Computational Materials Science*, Vol. 138, pp. 419–425, 2017.

83. Xia, Y., "Revisiting lattice thermal transport in PbTe: The crucial role of quartic anharmonicity", *Applied Physics Letters*, Vol. 113, No. 7, pp. 1–5, 2018.

84. Zou, J., D. Kotchetkov, A. A. Balandin, D. I. Florescu and F. H. Pollak, "Thermal conductivity of GaN films: Effects of impurities and dislocations", *Journal of Applied Physics*, Vol. 92, No. 5, pp. 2534–2539, 2002.

85. Li, W., J. Carrete, N. A. Katcho and N. Mingo, "ShengBTE: A solver of the Boltzmann transport equation for phonons", *Computer Physics Communications*, Vol. 185, No. 6, pp. 1747–1758, 2014.

86. Mizokami, K., A. Togo and I. Tanaka, "Lattice thermal conductivities of two SiO2 polymorphs by first-principles calculations and the phonon Boltzmann transport equation", *Physical Review B*, Vol. 97, No. 22, pp. 1–10, 2018.

87. Santia, M. D., N. Tandon and J. D. Albrecht, "Lattice thermal conductivity in β - Ga 2 O 3 from first principles", *Applied Physics Letters*, Vol. 107, No. 4, pp. 1–4, 2015.

88. Togo, A. and I. Tanaka, "First principles phonon calculations in materials science", *Scripta Materialia*, Vol. 108, pp. 1–5, 2015.

89. Togo, A., L. Chaput and I. Tanaka, "Distributions of phonon lifetimes in Brillouin zones", *Physical Review B*, Vol. 91, No. 9, pp. 1–36, 2015.

90. Ma, J., X. Wang, B. Huang and X. Luo, "Effects of point defects and dislocations on spectral phonon transport properties of wurtzite GaN", *Journal of Applied Physics*, Vol. 114, No. 7, pp. 1–8, 2013.

91. Albar, I. and N. Donmezer, "Mean Free Path–Thermal Conductivity Accumulation Calculations for Wurtzite Gallium Nitride: Two Approaches", *Nanoscale and Microscale Thermophysical Engineering*, Vol. 24, No. 2, pp. 80–93, 2020.

92. Garg, J., T. Luo and G. Chen, "Spectral concentration of thermal conductivity in GaN - A first-principles study", *Applied Physics Letters*, Vol. 112, No. 25, pp. 1–5, 2018.

93. Donmezer, F. N. and S. Graham, "Phonon Mean Free Path and Thermal Conductivity Relation for Gallium Nitride", *Proceeding of First Thermal and Fluids Engineering Summer Conference*, pp. 1649–1655, Begellhouse, Connecticut, 2016.

94. Albar, I. and N. Donmezer, "Phonon Mean Free Path - Thermal Conductivity Relation in AlN", *18th IEEE Intersociety Conference on Thermal and Thermomechanical Phenomena in Electronic Systems (ITherm)*, Vol. 2019-May, pp. 127–

130, 2019.

95. Miwa, K. and A. Fukumoto, "First-principles calculation of the structural, electronic, and vibrational properties of gallium nitride and aluminum nitride", *Physical Review B*, Vol. 48, No. 11, pp. 7897–7902, 1993.

96. Fu, J. Q., T. L. Song, X. X. Liang and G. J. Zhao, "First-principle studies of phonons and thermal properties of AlN in wurtzite structure", *Journal of Physics: Conference Series*, Vol. 574, pp. 1–6, 2014.

97. Liu, W. and A. A. Balandin, "Thermal conduction in AlxGa1-xN alloys and thin films", *Journal of Applied Physics*, Vol. 97, No. 7, pp. 1–6, 2005.

98. Kresse, G. and M. Marsman, *Vasp Manual*, 2014, `https://www.vasp.at/wiki/`, Last accessed on 2020-07-05.

99. Kresse, G. and J. Hafner, "Ab initio molecular dynamics for liquid metals", *Physical Review B*, Vol. 47, No. 1, pp. 558–561, 1993.

100. Kresse, G. and J. Hafner, "Ab initio molecular-dynamics simulation of the liquid-metal amorphous semiconductor transition in germanium", *Physical Review B*, Vol. 49, No. 20, pp. 14251–14269, 1994.

101. Kresse, G. and J. Furthmüller, "Efficiency of ab-initio total energy calculations for metals and semiconductors using a plane-wave basis set", *Computational Materials Science*, Vol. 6, No. 1, pp. 15–50, 1996.

102. Kresse, G. and J. Furthmüller, "Efficient iterative schemes for ab initio total-energy calculations using a plane-wave basis set", *Physical Review B*, Vol. 54, No. 16, pp. 11169–11186, 1996.

103. Leszczynski, M., H. Teisseyre, T. Suski, I. Grzegory, M. Bockowski, J. Jun, S. Porowski, K. Pakula, J. M. Baranowski, C. T. Foxon and T. S. Cheng, "Lattice

parameters of gallium nitride", *Applied Physics Letters*, Vol. 69, No. 1, pp. 73–75, 1996.

104. Slack, G. A., L. J. Schowalter, D. Morelli and J. A. Freitas, "Some effects of oxygen impurities on AlN and GaN", *Journal of Crystal Growth*, Vol. 246, No. 3-4, pp. 287–298, 2002.

105. Jezowski, A., B. A. Danilchenko, M. Boćkowski, I. Grzegory, S. Krukowski, T. Suski and T. Paszkiewicz, "Thermal conductivity of GaN crystals in 4.2-300 K range", *Solid State Communications*, Vol. 128, No. 2-3, pp. 69–73, 2003.

106. Regner, K. T., D. P. Sellan, Z. Su, C. H. Amon, A. J. McGaughey and J. A. Malen, "Broadband phonon mean free path contributions to thermal conductivity measured using frequency domain thermoreflectance", *Nature Communications*, Vol. 4, No. 1, pp. 1–7, 2013.

107. Shahien, M., M. Yamada, T. Yasui and M. Fukumoto, "Cubic aluminum nitride coating through atmospheric reactive plasma nitriding", *Journal of Thermal Spray Technology*, Vol. 19, pp. 635–641, 2010.

108. Bajracharya, P., *Aluminium Nitride : an overview of the physical properties*, 2002, `http://www.phys.lsu.edu/Material_Reviews`, Last accessed on 2020-07-21.

109. Park, M. H. and S. H. Kim, "Thermal conductivity of AlN thin films deposited by RF magnetron sputtering", *Materials Science in Semiconductor Processing*, Vol. 15, No. 1, pp. 6–10, 2012.

110. Cho, J., E. Bozorg-Grayeli, D. H. Altman, M. Asheghi and K. E. Goodson, "Low thermal resistances at GaN-SiC interfaces for HEMT technology", *IEEE Electron Device Letters*, Vol. 33, No. 3, pp. 378–380, 2012.

111. Koh, Y. K., Y. Cao, D. G. Cahill and D. Jena, "Heat-transport mechanisms in superlattices", *Advanced Functional Materials*, Vol. 19, No. 4, pp. 610–615, 2009.

112. Zhu, W., G. Zheng, S. Cao and H. He, "Thermal conductivity of amorphous SiO2 thin film: A molecular dynamics study", *Scientific Reports*, Vol. 8, No. 1, pp. 1–9, 2018.

113. Wang, Z., F. Gao, J. P. Crocombette, X. T. Zu, L. Yang and W. J. Weber, "Thermal conductivity of GaN nanotubes simulated by nonequilibrium molecular dynamics", *Physical Review B - Condensed Matter and Materials Physics*, Vol. 75, No. 15, pp. 1–4, 2007.

114. Béré, A. and A. Serra, "Atomic structure of dislocation cores in GaN", *Physical Review B - Condensed Matter and Materials Physics*, Vol. 65, No. 20, pp. 1–10, 2002.

115. Béré, A. and A. Serra, "On the atomic structures, mobility and interactions of extended defects in GaN: Dislocations, tilt and twin boundaries", *Philosophical Magazine*, Vol. 86, pp. 2159–2192, 2006.